J. Math. Biol. (2009) 59:809–840
DOI 10.1007/s00285-009-0253-z

Mathematical Biology

Modelling crystal aggregation and deposition in the catheterised lower urinary tract

L. R. Band · L. J. Cummings · S. L. Waters · J. A. D. Wattis

Received: 5 December 2007 / Revised: 20 January 2009 / Published online: 27 February 2009

Abstract Urethral catheters often become encrusted with crystals of magnesium struvite and calcium phosphate. The encrustation can block the catheter, which can cause urine retention in the bladder and reflux into the kidneys. We develop a mathematical model to investigate crystal deposition on the catheter surface, modelling the bladder as a reservoir of fluid and the urethral catheter as a rigid channel. At a constant rate, fluid containing crystal particles of unit size enters the reservoir, and flows from the reservoir through the channel and out of the system. The crystal particles aggregate, which we model using Becker–Döring coagulation theory, and are advected through the channel, where they continue to aggregate and are deposited on the channel's walls. Inhibitor particles also enter the reservoir, and can bind to the crystals, preventing further aggregation and deposition. The crystal concentrations are spatially homogeneous in the reservoir, whereas the channel concentrations vary

L. R. Band (✉) · J. A. D. Wattis
School of Mathematical Sciences, University of Nottingham, Nottingham NG7 2RD, UK
e-mail: leah.band@nottingham.ac.uk

J. A. D. Wattis
e-mail: jonathan.wattis@nottingham.ac.uk

L. R. Band
Centre for Plant Integrative Biology, University of Nottingham, Sutton Bonington LE12 5RD, UK

L. J. Cummings
Department of Mathematical Sciences, New Jersey Institute of Technology,
University Heights, Newark, NJ 07102-1982, USA
e-mail: linda.j.cummings@njit.edu

S. L. Waters
Oxford Centre for Industrial and Applied Mathematics, Mathematical Institute,
24-29 St Giles', Oxford OX1 3LB, UK
e-mail: waters@maths.ox.ac.uk

spatially as a result of advection, diffusion and deposition. We investigate the effect of inhibitor particles on the amount of deposition. For all parameter values, we find that crystals deposit along the full length of the channel, with maximum deposition close to the channel's entrance.

Keywords Urethra · Bladder · Catheter · Encrustation · Blockage · Aggregation · Becker–Döring · Deposition · Fluid flow · Mathematical modelling

Mathematics Subject Classification (2000) 92C50

1 Introduction

In the urinary tract, urine is produced by the kidneys, flows down the ureters and is stored in the bladder (see Fig. 1). The urethra, which connects the bladder to the external environment, remains closed, except during voiding, when a rise in bladder pressure causes the urethra to open and the bladder urine to flow through the urethra and exit the body. Urethral catheters are used to manage incontinence, to relieve urine retention caused by urethral blockage, and to monitor urinary output in critically ill patients (Morris and Stickler 2001). These rigid latex tubes sit against the urethral wall and are secured by a balloon in the bladder. Bladder urine enters the catheter via an eyelet, and flows through the catheter's lumen at a constant rate of approximately 0.5–3 ml min^{-1} (Stickler and Morgan 2006; Morris and Stickler 2001). On exiting the catheter, the urine is collected in an external reservoir.

Although urethral catheters are widely used, they often become blocked. Catheter blockage can cause urine to leak around the outside of the catheter, or can cause urine retention in the bladder and reflux into the kidneys, which can lead to pyelonephritis, septicaemia, and even endotoxic shock (Morris et al. 1999; Suller 2005; Morris and Stickler 1998). To avoid these complications, urethral catheters currently need to be replaced regularly (Morris and Stickler 1998). Reducing catheter blockage therefore has the potential to improve the efficacy of clinical procedures and patient experience.

Catheter blockage is caused by encrustation on the catheter's surface. Soon after insertion, bacteria such as *Proteus mirabilis* colonise the catheter surface and form a biofilm consisting of communities of bacterial cells within an exopolysaccharide matrix (Suller 2005; Stickler and Morgan 2006). Within a few days, the bacteria traverse the length of the catheter, and are present in the bladder urine. The bacteria produce urease, which catalyses the hydrolysis of urea in the urine, and this reaction produces ammonia, which elevates the pH within the biofilm and in the bulk urine (Clapham et al. 1990; Suller 2005; Mathur et al. 2006). In the resulting alkaline environments, crystals of magnesium struvite and calcium phosphate form. In the bulk urine, the crystals aggregate, and can be deposited on the catheter's surface and become trapped in the biofilm (Stickler and Morgan 2006; Suller 2005). The resulting catheter surface encrustation can eventually block the catheter's lumen (Burr and Nuseibeh 1997; Morris and Stickler 1998; Stickler and Morgan 2006; Suller 2005).

Several studies have investigated methods to reduce the degree of catheter encrustation. Burr and Nuseibeh (1997) studied the urinary output of catheterised patients

and found less catheter encrustation in patients who maintained a high and uniform fluid intake. A related in vitro model of the catheterised lower urinary tract showed that increasing the flux through the catheter by diluting the urine reduced the degree of catheter encrustation, whereas increasing the flux without diluting the urine did not affect the degree of encrustation (Stickler and Morgan 2006; Morris and Stickler 2001). As well as maintaining a high fluid intake, patients are also encouraged to increase the amount of citrate in their diets (Morris and Stickler 2001). Increasing the citrate concentration of urine (within the physiological range) has been shown to reduce crystal growth for both magnesium struvite and calcium phosphate (Wang et al. 1993; Wierzbicki et al. 1997); however, studies on citrate's influence on catheter encrustation have produced conflicting results (Stickler and Morgan 2006; Morris and Stickler 2001).

Current literature suggests that the encrusted layer grows due to two mechanisms: (i) by crystals forming within the biofilm; and (ii) by crystals forming in the surrounding urine, being deposited onto the catheter, and then incorporated into the biofilm. The relative importance of the two mechanisms remains unclear. A recent mathematical model (J.H. Siggers, J.A.D. Wattis, L.J. Cummings and S.L. Waters, paper in preparation), focuses on the crystals that develop in the biofilm and assumes that these crystals form a solid layer next to the catheter surface. Here we focus on the crystals that aggregate in the bulk urine and deposit on the catheter surface. We ignore the biofilm except insofar as it leads to crystal aggregation in the bulk urine via an increase in pH. We use our model to investigate how aggregation and the presence of inhibitor particles (for example, citrate) affect the amount of deposition. We assume that crystal particles of unit size (monomers) and inhibitor particles are advected into the bladder from the ureters at a constant rate. In the bladder, crystals grow by the addition of monomers, which is appropriate for the slow crystal growth seen experimentally (McLean et al. 1991). We suppose that crystal clusters do not fragment, and that crystals can be 'poisoned' by the inhibitor particles, which prevents further aggregation and deposition. The crystals and inhibitor particles are advected out of the bladder through the rigid catheter, where they diffuse and aggregate in the bulk urine and deposit on the catheter's surface.

We model crystal aggregation using the pure aggregation form of the Becker–Döring equations (Becker and Döring 1935), which model reactions occurring between monomers and clusters. The Becker–Döring model is the basis for classical nucleation theory, which assumes that interactions between monomers and clusters are the dominant growth mechanism, and ignores cluster-cluster interactions. The Becker–Döring model is a special case of Smoluchowski coagulation theory (Smoluchowski 1916), which more generally allows all cluster sizes to aggregate, and clusters to split into uneven fragments. Coagulation theory has been used extensively to model aggregation in numerous situations [for a review see Wattis (2006) and references therein]. Of particular interest here are recent models which combine inhibition with Becker–Döring kinetics (Bolton and Wattis 2004; Wattis and Coveney 1997). Despite a wide literature on coagulation theory, little attention has been paid to spatially varying cluster concentrations. Smoluchowski coagulation theory with diffusion was formulated by Slemrod (1990) (among others) and explicit analytical solutions in special cases have been identified (Herrero and Rodrigo 2005; Simons 1992, 1996); Becker–Döring kinet-

ics with diffusing particles have also been studied (Laurencot and Wrzosek 1998). Although coupling coagulation theory with the Navier–Stokes equations is mathematically well-posed (Amann and Weber 2001), only a few models have combined advection, aggregation and diffusion, notable examples being the work of Guy et al. (2007), who modelled the formation of a blood clot in a shear flow, and Fozard and King (2008), who studied cell aggregation in the presence of a chemotactic signal (which creates an advective motion). As far as we are aware, no previous work has incorporated either Becker–Döring or Smoluchowski coagulation theory into an advection-diffusion model where cluster concentrations vary in two spatial dimensions.

In Sect. 2, we present the model, derive the governing equations and discuss the physiological parameter values appropriate for modelling urethral catheter encrustation. Based on the available parameter estimates, we focus on a large aggregation rate and determine how the relative rates at which inhibitor particles and monomers enter the bladder influence the degree of encrustation, considering the bladder dynamics in Sect. 3 and the catheter dynamics in Sect. 4. In Sect. 5, we summarise our results and discuss possible model extensions.

2 Model

As shown in Fig. 1, we consider a two-dimensional model and consider the bladder to be a reservoir of fluid, which flows through a rigid channel (the catheter) of length L^* and width $2Y^*$ (we use asterisks throughout to denote dimensional quantities). We assume that the reservoir fluid is well-mixed, whereas in the channel, we consider spatial dependence, and use a Cartesian coordinate system (x^*, y^*). To maintain a constant reservoir volume, fluid enters the reservoir through two channels (which represent the ureters). Due to this influx, monomers and inhibitor particles enter the reservoir at rates Q_1^* and H^* per unit area respectively. The monomers aggregate to form clusters.

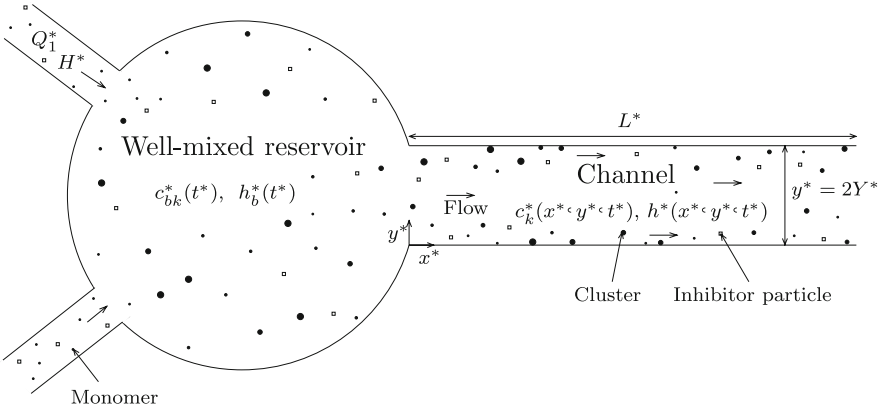

Fig. 1 We model the bladder as reservoir of fluid and the catheterised urethra as a two-dimensional rigid channel. At a constant rate, urine from the kidneys enters the bladder via the two ureters, and the bladder urine flows through the urethra and exits the body

In the well-mixed reservoir fluid, the spatially homogeneous bulk concentrations of monomers, clusters of $k \geq 2$ particles (k-clusters) and inhibitor particles are denoted respectively by $c^*_{b1}(t^*)$, $c^*_{bk}(t^*)$ and $h^*_b(t^*)$, where t^* denotes time and bulk concentration refers to the number per unit area. We assume that the bulk concentrations are sufficiently small that we need only consider binary aggregation. The monomers and inhibitor particles aggregate with monomers and clusters with rate coefficient A^*, which has dimensions $\mathrm{m^2 s^{-1}}$. To maintain analytical tractability, we assume that the aggregation rate is independent of cluster size and that the clusters do not fragment. Interactions between monomers and clusters are the dominant crystal growth mechanism (McLean et al. 1991), and therefore we suppose that there is no aggregation between clusters of arbitrary size. We assume that binding with an inhibitor particle prevents further aggregation; the monomers and clusters are then considered to be poisoned, and are of no further interest.

The contents of the well-mixed reservoir fluid are advected into the channel at rate λ^*. In the channel, the bulk concentrations of monomers, k-clusters and inhibitor particles vary spatially and are denoted by $c^*_1(x^*, y^*, t^*)$, $c^*_k(x^*, y^*, t^*)$ and $h^*(x^*, y^*, t^*)$ respectively. The monomers, clusters and inhibitor particles are advected by the flow and diffuse. We suppose that the diffusion coefficient, D^*, is independent of cluster size; although larger clusters will in reality have a smaller diffusion coefficient, we assume that the variations in the clusters' sizes are sufficiently small that differences in the diffusion coefficients will not qualitatively change the model predictions. We assume that the aggregation dynamics and rate coefficients in the channel are identical to those in the reservoir.

At the channel walls, $y^* = 0$ and $y^* = 2Y^*$, monomers and clusters are deposited at a rate proportional to their bulk concentrations, with rate coefficient α^*, which has dimensions $\mathrm{m\,s^{-1}}$. We assume that the deposited monomers and clusters do not interact with the monomers and clusters present in the bulk fluid, and so do not affect the deposition rate, α^*. We denote the surface concentrations of deposited monomers and k-clusters by $s^*_1(x^*, t^*)$ and $s^*_k(x^*, t^*)$ respectively (for $k \geq 2$), where surface concentration refers to the number per unit length. In a urethral catheter, deposited crystals become trapped in the developing biofilm; we therefore assume that deposited monomers and clusters remain on the wall and cannot be poisoned by inhibitor particles. For simplicity, we also suppose that the inhibitor particles and poisoned clusters are not deposited on the channel walls.

We focus on the early stages of catheter encrustation and assume that the deposited crystal layer is thin relative to the channel width, so that the channel width is constant, and the crystal layer does not influence the fluid dynamics. We suppose that the pressure difference between the reservoir and the external environment is constant, denoted P^*; therefore, assuming Poiseuille flow, the axial velocity is given by $P^* y^* (2Y^* - y^*)/(2L^* \eta^*)$ where η^* is the fluid's dynamic viscosity. [We note that the flow's development length is small relative to the channel length (Durst 2005) and is neglected for simplicity.]

We assume symmetry in the channel's centre line, $y^* = Y^*$, and solve on the domain $y^* \in [0, Y^*]$. We suppose that initially there are no monomers, clusters or inhibitor particles present in the reservoir or channel (as the system will have been flushed when the catheter is inserted). Monomers and inhibitor particles are introduced

into the reservoir (the bladder) from $t^* = 0$ onwards, and we consider the dynamics as a result of crystals aggregating in the urine and depositing on the catheter.

2.1 Governing equations and boundary conditions

In the well-mixed reservoir, the bulk concentrations of monomers, clusters and inhibitor particles are governed by

$$\frac{\mathrm{d}c_{b1}^*}{\mathrm{d}t^*} = Q_1^* - \lambda^* c_{b1}^* - A^* c_{b1}^{*2} - A^* c_{b1}^* h_b^* - A^* c_{b1}^* \sum_{j=1}^{\infty} c_{bj}^*, \tag{2.1a}$$

$$\frac{\mathrm{d}c_{bk}^*}{\mathrm{d}t^*} = -\lambda^* c_{bk}^* + A^* c_{b(k-1)}^* c_{b1}^* - A^* c_{bk}^* c_{b1}^* - A^* c_{bk}^* h_b^* \quad \text{for}\, k > 1, \tag{2.1b}$$

$$\frac{\mathrm{d}h_b^*}{\mathrm{d}t^*} = H^* - \lambda^* h_b^* - A^* h_b^* \sum_{j=1}^{\infty} c_{bj}^*. \tag{2.1c}$$

The bulk concentrations change due to monomers and inhibitor particles entering the reservoir (the first terms on the right-hand sides of (2.1a,c)), their flux out of the reservoir (the first term on the right-hand side of (2.1b), and the second terms on the right-hand sides of (2.1a,c)), and aggregation (the remaining terms). In the channel, the bulk concentrations of monomers, clusters and inhibitor particles are governed by

$$\frac{\partial c_1^*}{\partial t^*} = D^* \left(\frac{\partial^2 c_1^*}{\partial x^{*2}} + \frac{\partial^2 c_1^*}{\partial y^{*2}} \right) - \frac{P^*}{L^* \eta^*} y^* \left(Y^* - \frac{y^*}{2} \right) \frac{\partial c_1^*}{\partial x^*} - A^* c_1^{*2} - A^* c_1^* h^* - A^* c_1^* \sum_{j=1}^{\infty} c_j^*, \tag{2.2a}$$

$$\frac{\partial c_k^*}{\partial t^*} = D^* \left(\frac{\partial^2 c_k^*}{\partial x^{*2}} + \frac{\partial^2 c_k^*}{\partial y^{*2}} \right) - \frac{P^*}{L^* \eta^*} y^* \left(Y^* - \frac{y^*}{2} \right) \frac{\partial c_k^*}{\partial x^*} + A^* c_{k-1}^* c_1^* - A^* c_k^* c_1^* - A^* c_k^* h^* \quad \text{for} \quad k > 1, \tag{2.2b}$$

$$\frac{\partial h^*}{\partial t^*} = D^* \left(\frac{\partial^2 h^*}{\partial x^{*2}} + \frac{\partial^2 h^*}{\partial y^{*2}} \right) - \frac{P^*}{L^* \eta^*} y^* \left(Y^* - \frac{y^*}{2} \right) \frac{\partial h^*}{\partial x^*} - A^* h^* \sum_{j=1}^{\infty} c_j^*, \tag{2.2c}$$

where the first terms on the right-hand sides of (2.2) model diffusion, the second terms model advection and the remaining terms model aggregation.

We solve equations (2.2) subject to the following boundary conditions. We suppose that the bulk concentrations are continuous at the channel entrance and do not change as the monomers, clusters and inhibitor particles exit the channel, therefore

$$c_k^* = c_{bk}^*, \qquad h^* = h_b^* \quad \text{at} \quad x^* = 0, \qquad \frac{\partial c_k^*}{\partial x^*} = \frac{\partial h^*}{\partial x^*} = 0 \quad \text{at} \quad x^* = L^*, \tag{2.3a,b}$$

(for $k \geq 1$). Symmetry in the channel's centre line requires that

$$\frac{\partial c_k^*}{\partial y^*} = \frac{\partial h^*}{\partial y^*} = 0 \quad \text{for } k \geq 1 \quad \text{at } y^* = Y^*. \tag{2.4}$$

At the channel wall, the monomers and clusters deposit at a rate proportional to their bulk concentrations, and the inhibitor particles do not deposit, so that

$$D^* \frac{\partial c_k^*}{\partial y^*} = \alpha^* c_k^*, \quad \frac{\partial h^*}{\partial y^*} = 0 \quad \text{for } k \geq 1 \quad \text{at } y^* = 0. \tag{2.5a,b}$$

Thus, the surface concentrations of deposited monomers and clusters are governed by

$$\frac{\partial s_k^*}{\partial t^*} = \alpha^* c_k^* \quad \text{for } k \geq 1 \quad \text{at } y^* = 0. \tag{2.6}$$

We assume that initially there are no monomers, clusters or inhibitor particles present in the reservoir or the channel.

2.2 Nondimensionalisation

We consider the dynamics on the time scale $1/\lambda^*$ over which the monomers, clusters and inhibitor particles leave the reservoir and enter the channel. We nondimensionalise using

$$t^* = \frac{t}{\lambda^*}, \quad x^* = L^* x, \ \ y^* = Y^* y,$$
$$(c_{bk}^*, h_b^*, c_k^*, h^*) = \frac{Q_1^*}{\lambda^*}(c_{bk}, h_b, c_k, h), \quad s_k^* = \frac{Y^* Q_1^*}{\lambda^*} s_k,$$

for $k \geq 1$, and identify six dimensionless parameters,

$$\epsilon = \frac{Y^*}{L^*}, \quad A = \frac{Q_1^* A^*}{\lambda^{*2}}, \quad H = \frac{H^*}{Q_1^*}, \quad P = \frac{P^* Y^{*2}}{L^{*2} \eta^* \lambda^*}, \quad D = \frac{D^*}{Y^{*2} \lambda^*}, \quad \alpha = \frac{\alpha^*}{Y^* \lambda^*}.$$

The aspect ratio based on the channel half width is denoted by ϵ. The parameter A is the ratio between the aggregation rate and the rate at which monomers, clusters and inhibitor particles enter the channel. The parameter H is the ratio between the rates at which inhibitor particles and monomers enter the reservoir. The parameter P gives the ratio between the rate at which monomers, clusters and inhibitor particles are advected a distance L^*, and the rate at which they enter the channel, and the parameter D gives the ratio between the rate at which monomers, clusters and inhibitor particles diffuse a distance Y^*, and the rate at which they enter the channel. Finally, the ratio between the deposition rate and the rate at which monomers, clusters and inhibitor particles enter the channel is given by α.

The model is governed by an infinite number of equations, (2.1, 2.2, 2.6), for an infinite number of variables. For ease, we reduce the number of variables to eleven: $c_{b1}(t)$, $c_1(x, y, t)$, $s_1(x, t)$, $h_b(t)$, $h(x, y, t)$, and

$$n_b(t) = \sum_{k=2}^{\infty} c_{bk}(t), \quad n(x, y, t) = \sum_{k=2}^{\infty} c_k(x, y, t), \quad n_s(x, t) = \sum_{k=2}^{\infty} s_k(x, t),$$
$$m_b(t) = \sum_{k=1}^{\infty} k c_{bk}(t), \quad m(x, y, t) = \sum_{k=1}^{\infty} k c_k(x, y, t), \quad m_s(x, t) = \sum_{k=1}^{\infty} k s_k(x, t).$$

Thus, the bulk cluster concentrations are $n_b(t)$ and $n(x, y, t)$, and the total mass of monomers and clusters per unit area are $m_b(t)$ and $m(x, y, t)$ in the reservoir and in the channel respectively.[1] At the channel wall, the surface cluster concentration is $n_s(x, t)$, and the total mass of monomers and clusters per unit length is $m_s(x, t)$. We can then determine properties of the system in terms of these eleven variables, for example, the typical cluster size in the channel (including the monomers) is given by $m/(c_1 + n)$.

From (2.1, 2.2, 2.6), the reduced system of governing equations is

$$\frac{\mathrm{d}c_{b1}}{\mathrm{d}t} = 1 - c_{b1} - 2Ac_{b1}^2 - Ac_{b1}n_b - Ac_{b1}h_b, \tag{2.7a}$$
$$\frac{\mathrm{d}n_b}{\mathrm{d}t} = -n_b + Ac_{b1}^2 - An_bh_b, \tag{2.7b}$$
$$\frac{\mathrm{d}h_b}{\mathrm{d}t} = H - h_b - Ac_{b1}h_b - An_bh_b, \tag{2.7c}$$
$$\frac{\mathrm{d}m_b}{\mathrm{d}t} = 1 - m_b - Am_bh_b, \tag{2.7d}$$
$$\frac{\partial c_1}{\partial t} = D\left(\epsilon^2\frac{\partial^2 c_1}{\partial x^2} + \frac{\partial^2 c_1}{\partial y^2}\right) - Py\left(1 - \frac{y}{2}\right)\frac{\partial c_1}{\partial x} - 2Ac_1^2 - Ac_1n - Ac_1h, \tag{2.7e}$$
$$\frac{\partial n}{\partial t} = D\left(\epsilon^2\frac{\partial^2 n}{\partial x^2} + \frac{\partial^2 n}{\partial y^2}\right) - Py\left(1 - \frac{y}{2}\right)\frac{\partial n}{\partial x} + Ac_1^2 - Anh, \tag{2.7f}$$
$$\frac{\partial h}{\partial t} = D\left(\epsilon^2\frac{\partial^2 h}{\partial x^2} + \frac{\partial^2 h}{\partial y^2}\right) - Py\left(1 - \frac{y}{2}\right)\frac{\partial h}{\partial x} - Ac_1h - Anh, \tag{2.7g}$$
$$\frac{\partial m}{\partial t} = D\left(\epsilon^2\frac{\partial^2 m}{\partial x^2} + \frac{\partial^2 m}{\partial y^2}\right) - Py\left(1 - \frac{y}{2}\right)\frac{\partial m}{\partial x} - Amh, \tag{2.7h}$$
$$\frac{\partial s_1}{\partial t} = \alpha c_1, \quad \frac{\partial n_s}{\partial t} = \alpha n, \quad \frac{\partial m_s}{\partial t} = \alpha m \quad \text{at} \quad y = 0. \tag{2.7i}$$

The corresponding boundary conditions (2.3–2.5), become

$$c_1 = c_{b1}, \quad n = n_b, \quad h = h_b, \quad m = m_b \quad \text{at} \quad x = 0, \tag{2.8a}$$

[1] For ease, we state the mass with units corresponding to the mass of one monomer.

Table 1 Physiological estimates of the dimensional parameters required by the model. We justify these parameter choices and provide references in Appendix A

Parameter	Description	Value
L^*	Catheter length	0.20 m
Y^*	Catheter width	$0.008/\pi$ m
η^*	Urine dynamic viscosity	0.654×10^{-3} kg m^{-1} s^{-1}
P^*	Pressure difference across catheter	0.050 Pa
λ^*	Rate at which urine leaves bladder	3×10^{-5} s^{-1}
Q_1^*	Monomer input	2×10^{20} m^{-3} s^{-1}
H^*/Q_1^*	Relative inhibitor-particle input	[0, 2]
D^*	Diffusion rate	7×10^{-10} m^2 s^{-1}
A^*	Aggregation rate	8.7×10^{-18} m^3 s^{-1}

$$\frac{\partial c_1}{\partial x} = \frac{\partial n}{\partial x} = \frac{\partial h}{\partial x} = \frac{\partial m}{\partial x} = 0 \quad \text{at } x = 1, \tag{2.8b}$$

$$D\frac{\partial c_1}{\partial y} = \alpha c_1, \quad D\frac{\partial n}{\partial y} = \alpha n, \quad \frac{\partial h}{\partial y} = 0, \quad D\frac{\partial m}{\partial y} = \alpha m \quad \text{at } y = 0, \tag{2.8c}$$

$$\frac{\partial c_1}{\partial y} = \frac{\partial n}{\partial y} = \frac{\partial h}{\partial y} = \frac{\partial m}{\partial y} = 0 \quad \text{at } y = 1, \tag{2.8d}$$

and the initial conditions become

$$c_{b1} = n_b = h_b = m_b = c_1 = n = h = m = s_1 = n_s = m_s = 0 \quad \text{at } t = 0. \tag{2.9}$$

To summarise, we prescribe the six dimensionless parameters, ϵ, A, H, D, P and α, and solve the governing equations, (2.7), for the eleven variables, subject to the boundary conditions (2.8) and the initial conditions (2.9).

2.3 Physiological parameter values

Physiologically relevant parameter estimates are discussed in Appendix A and summarised in Table 1. These values lead to the following estimates for some of the dimensionless parameters

$$\epsilon = 0.013, \quad A = 2 \times 10^{12}, \quad H = 0 - 2, \quad P = 410, \quad D = 3.6. \tag{2.10}$$

The deposition rate, α, will depend strongly on the biomaterial properties of the catheter and on the extent of the bacterial biofilm. We therefore use the model to investigate the impact of different deposition rates.

We focus on the physiologically relevant solutions for which the dimensionless aggregation rate is large, $A \gg 1$, and motivated by (2.10), we suppose that the parameters, H and D are $O(1)$ as $A \to \infty$. When we asymptotically study the channel solutions in Sects. 4.1.3 and 4.2.3, we find that the dominant dynamics

depend on the relative sizes of ϵ, P and $A^{-1/4}$ for $H > 1$ and ϵ, P and $A^{-1/8}$ for $0 < H < 1$; considering the physiological parameter estimates, (2.10), we let $A^{-1/4} \ll \epsilon \sim P^{-1} \ll A^{-1/8}$.

Studying the reservoir solutions in Sect. 3, we focus on varying the input of inhibitor particles, $H \in [0, 2]$. We then consider the channel dynamics in Sect. 4, and present both time-dependent numerical solutions and asymptotic steady solutions. We investigate the dynamics both with no deposition, $\alpha = 0$, and with sufficiently fast deposition that its influence on the bulk concentrations can be clearly seen.

3 Reservoir solutions

For large A, the appropriate asymptotic scalings for the steady-state bulk concentrations depend upon H, the ratio between the rates at which inhibitor particles and monomers enter the reservoir. Considering the four asymptotic regimes, $H > 1$, $0 < H < 1$, $H \approx 1$ and $H \approx 0$, we determine steady reservoir solutions in Sect. 3.1 and discuss dynamics effects in Sect. 3.2.

3.1 Asymptotic steady-state solutions

In Sects. 3.1.1–3.1.4, we discuss the steady solutions of (2.7a-d) in four asymptotic regimes: $H > 1, 0 < H < 1, H \approx 1$ and $H \approx 0$. In each case, we obtain the appropriate asymptotic scalings for c_{b1}, n_b, h_b and m_b, by seeking a consistent balance in the steady-state governing equations (ensuring that the bulk concentrations are positive).

3.1.1 Inhibitor input $H > 1$

For $H > 1$, the appropriate asymptotic scalings are

$$(c_{b1}, m_b) = A^{-1}(\tilde{c}_{b1}, \tilde{m}_b), \quad n_b = A^{-2}\tilde{n}_b. \tag{3.1a,b}$$

As the inhibitor-particle input exceeds the monomer input, the inhibitor-particle concentration is larger than the concentrations of monomers and clusters. The monomer concentration is much larger than the cluster concentration and the mass is predominantly due to the monomers, because many of the monomers are poisoned before they form clusters. At leading order, the steady-state governing equations (2.7a-d), become

$$\begin{aligned} 0 &= 1 - \tilde{c}_{b1}h_b, & 0 &= \tilde{c}_{b1}^2 - \tilde{n}_b h_b, \\ 0 &= H - h_b - \tilde{c}_{b1}h_b, & 0 &= 1 - \tilde{m}_b h_b. \end{aligned} \tag{3.2a-d}$$

As the inhibitor-particle concentration is large, the input of monomers and formation of clusters is balanced with poisoning. We obtain the solution

$$c_{b1} = m_b = \frac{1}{A(H-1)}, \quad n_b = \frac{1}{A^2(H-1)^3}, \quad h_b = H - 1, \tag{3.3a-c}$$

and the leading-order typical cluster size, $m_b/(c_{b1} + n_b)$, equals one.

3.1.2 Inhibitor input $0 < H < 1$

For $0 < H < 1$, the concentrations of monomers, clusters and inhibitor particles all have the same asymptotic scaling:

$$(c_{b1}, n_b, h_b, m_b) = A^{-1/2}(\hat{c}_{b1}, \hat{n}_b, \hat{h}_b, \hat{m}_b), \tag{3.4}$$

and so both the monomers and the clusters contribute to the leading-order mass. The leading-order steady-state governing equations are

$$\begin{aligned} 0 &= 1 - 2\hat{c}_{b1}^2 - \hat{c}_{b1}\hat{n}_b - \hat{c}_{b1}\hat{h}_b, \quad & 0 &= \hat{c}_{b1}^2 - \hat{n}_b\hat{h}_b, \\ 0 &= H - \hat{c}_{b1}\hat{h}_b - \hat{n}_b\hat{h}_b, & 0 &= 1 - \hat{m}_b\hat{h}_b. \end{aligned} \tag{3.5a-d}$$

In this case, the input of monomers and inhibitor particles into the reservoir is balanced by aggregation and poisoning, and the flux of monomers, clusters and inhibitor particles out of the reservoir into the channel does not affect the leading-order reservoir solution. Equations (3.5) have solution

$$\begin{aligned} c_{b1} &= \frac{(H(1-H))^{1/2}}{A^{1/2}}, \quad & n_b &= \frac{(1-H)^{3/2}}{A^{1/2}H^{1/2}}, \\ h_b &= \frac{H^{3/2}}{A^{1/2}(1-H)^{1/2}}, & m_b &= \frac{(1-H)^{1/2}}{A^{1/2}H^{3/2}}, \end{aligned} \tag{3.6a-d}$$

and the leading-order typical cluster size is $m_b/(c_{b1} + n_b) = 1/H$.

3.1.3 Inhibitor input $H \approx 1$

Inspection of (3.3) and (3.6) reveals singularities as $H \to 1^{\pm}$. We therefore consider an inner region where $H \approx 1$; we let $H = 1 + A^{-1/3}\bar{H}$, where $\bar{H} = O(1)$ as $A \to \infty$, and rescale via

$$(c_{b1}, m_b) = A^{-2/3}(\bar{c}_{b1}, \bar{m}_b), \quad n_b = A^{-1}\bar{n}_b, \quad h_b = A^{-1/3}\bar{h}_b. \tag{3.7}$$

We obtain these scalings by prescribing that the solution will match to the $H < 1$ solution as $\tilde{H} \to -\infty$ and the $H > 1$ solution as $\tilde{H} \to \infty$. At leading order, the steady-state governing equations reduce to the system

$$\begin{aligned} 0 &= 1 - \bar{c}_{b1}\bar{h}_b, \quad & 0 &= \bar{c}_{b1}^2 - \bar{n}_b\bar{h}_b, \\ 0 &= \bar{H} - \bar{h}_b + \bar{c}_{b1}^2, & 0 &= 1 - \bar{m}_b\bar{h}_b, \end{aligned} \tag{3.8a-d}$$

(as $1 - \bar{c}_{b1}\bar{h}_b = 2\bar{c}_{b1}^2 A^{1/3} + \cdots$). Comparing (3.2) and (3.8), we see that the governing equations for $H > 1$ and $H \approx 1$ are essentially the same, although for $H \approx 1$ we solve for the inhibitor-particle concentration at a higher order (as Sect. 3.1.1 suggested that the $O(1)$ component of the inhibitor-particle concentration is zero if $H = 1$). Equations (3.8) simplify to

$$\bar{n}_b = \bar{c}_{b1}^3, \quad \bar{h}_b = \frac{1}{\bar{c}_{b1}}, \quad \bar{m}_b = \bar{c}_{b1}, \quad \bar{c}_{b1}^3 + \bar{H}\bar{c}_{b1} - 1 = 0, \tag{3.9a-d}$$

and the real root of the cubic for $\bar{c}_{b1}$, (3.9d), is given by

$$\bar{c}_{b1} = 2^{-1/3}\left((u+1)^{1/3} - (u-1)^{1/3}\right) \quad \text{where } u^2 = 1 + \frac{4\bar{H}^3}{27}. \tag{3.10}$$

For large $\bar{H}$, $u \sim 2(\bar{H}/3)^{3/2}$ and it is straightforward to show that $\bar{c}_{b1} \sim \bar{H}^{-1}$. Letting $\bar{H} = (H-1)A^{1/3}$, we find that the solution for large $\bar{H}$ is identical to the outer solution ($H > 1$), given in (3.3). Therefore, (3.10) holds for $H \gtrapprox 1$, and the $H > 1$ solution is redundant. In the limit $\bar{H} \to -\infty$, u takes complex values, and we let $u = iv$ where $v = 2(-\bar{H}/3)^{3/2} \in \mathbb{R}$. We then find that $\bar{c}_{b1} \sim (-\bar{H})^{1/2}$ as $\bar{H} \to -\infty$, so that

$$c_{b1} = m_b = \frac{(1-H)^{1/2}}{A^{1/2}}, \quad n_b = \frac{(1-H)^{3/2}}{A^{1/2}}, \quad h_b = \frac{1}{A^{1/2}(1-H)^{1/2}}. \tag{3.11}$$

Comparing (3.6) and (3.11), we see that the solution in the limit $\bar{H} \to -\infty$ is not identically equal to the outer solution ($0 < H < 1$). Rather, in the limit as $\bar{H} \to -\infty$, (3.11) matches to the outer solution in the limit $H \to 1^-$ (3.6).

3.1.4 Inhibitor input $H \approx 0$

In the solution for $0 < H < 1$, (3.6), the cluster concentration is singular as $H \to 0^+$; therefore, we now construct an asymptotic solution for $H \approx 0$. We let $H = A^{-1/3}\breve{H}$, where $\breve{H} = O(1)$ as $A \to \infty$; this scaling ensures we match to the $H < 1$ solution, (3.6), as $\breve{H} \to \infty$. We rescale via

$$c_{b1} = A^{-2/3}\breve{c}_{b1}, \quad n_b = A^{-1/3}\breve{n}_b, \quad h_b = A^{-1}\breve{h}_b. \tag{3.12}$$

The inhibitor-particle concentration is small and poisoning occurs slowly, resulting in the total mass of monomers and clusters being $O(1)$. Many of the monomers form clusters before they are poisoned, so that the cluster concentration is larger than the monomer concentration and the typical cluster size is $O(A^{1/3})$. The leading-order terms in the steady-state governing equations are

$$\begin{aligned} 0 &= 1 - \breve{c}_{b1}\breve{n}_b, \quad & 0 &= -\breve{n}_b + \breve{c}_{b1}^2 - \breve{n}_b\breve{h}_b, \\ 0 &= \breve{H} - \breve{n}_b\breve{h}_b, \quad & 0 &= 1 - m_b - m_b\breve{h}_b, \end{aligned} \tag{3.13a-d}$$

which can be simplified to

$$\breve{n}_b = \frac{1}{\breve{c}_{b1}}, \quad \breve{h}_b = \breve{H}\breve{c}_{b1}, \quad m_b = \frac{1}{1+\breve{H}\breve{c}_{b1}}, \quad \breve{c}_{b1}^3 - \breve{H}\breve{c}_{b1} - 1 = 0, \tag{3.14a-d}$$

where the cubic equation for $\breve{c}_{b1}$, (3.14d), has the unique real solution

$$\breve{c}_{b1} = 2^{-1/3}\left((u+1)^{1/3} - (u-1)^{1/3}\right) \quad \text{where} \quad u^2 = 1 - \frac{4\breve{H}^3}{27}. \tag{3.15}$$

In the limit as $\breve{H} \to \infty$, u takes complex values; we let $u = iv$ where $v = 2(\breve{H}/3)^{3/2} \in \mathbb{R}$ and find that $\breve{c}_{b1} \sim (\breve{H})^{1/2}$. Returning to unscaled concentrations, we obtain

$$c_{b1} = \frac{H^{1/2}}{A^{1/2}}, \quad n_b = \frac{1}{H^{1/2}A^{1/2}}, \quad h_b = \frac{H^{3/2}}{A^{1/2}}, \quad m_b = \frac{1}{H^{3/2}A^{1/2}}, \tag{3.16}$$

and so the limit as $\breve{H} \to \infty$ is consistent with the limit $H \to 0^+$ of the outer solution, (3.6).

3.1.5 Summary of the steady solutions

In summary, we have three asymptotic regions for H: $H \approx 0$, $0 < H < 1$ and $H \gtrapprox 1$. In Fig. 2, we compare the asymptotic steady-state solutions, obtained in Sect. 3.1.1–3.1.4, with large-time numerical solutions of the governing equations (2.7a-d). (The steady state is reached by $t = 5$.) The numerical solutions are produced by solving (2.7a-d) with initial conditions (2.9), using MATLAB's differential equation solver *ode45* (which uses a fourth-order accurate Runge–Kutta method). For $A = 5{,}000$, there is excellent agreement between the numerical solutions at large times and the asymptotic steady-state solutions.

Increasing the rate at which inhibitor particles enter the reservoir increases the inhibitor-particle concentration (Fig. 2c), and reduces the cluster concentration (Fig. 2b) (as more clusters are poisoned). From (3.6), the monomer concentration increases with H for $H < 0.5$, and decreases with H for $H > 0.5$ (Fig. 2a). There are two competing effects: increasing the inhibitor-particle concentration reduces the number of clusters for the monomers to aggregate with, which increases the monomer concentration and is the dominant effect for $H < 0.5$; however, increasing the inhibitor-particle concentration also increases the number of monomers poisoned, which reduces the monomer concentration, and is the dominant effect for $H > 0.5$.

With no inhibitor particles, the mass per unit area equals one. The mass reduces as the input of inhibitor particles increases (Fig. 2d), and more of the monomers and clusters become poisoned. Although not studied here, we would expect the mass of poisoned monomers and clusters to increase with H. For $H \gtrapprox 1$, many monomers are poisoned before they can aggregate with clusters, so the typical cluster size is small (approximately equal to one) and the leading-order mass is entirely due to the monomers, $m_b = c_{b1}$. Therefore, the reservoir contains predominantly monomers and inhibitor particles. For $H < 1$, the typical cluster size increases with decreasing H (Fig. 2e), and monomers, clusters and inhibitor particles are all present in the reservoir.

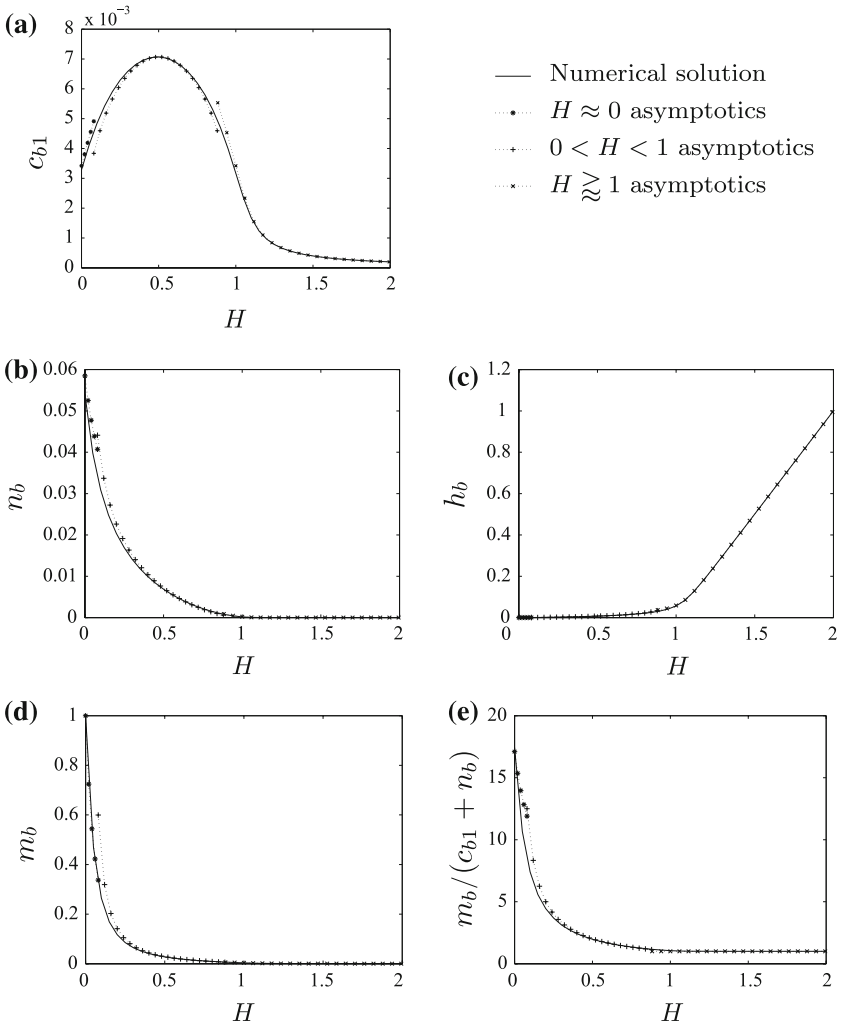

Fig. 2 Influence of the ratio between the rates at which inhibitor particles and monomers enter the reservoir, H, on the steady-state bulk concentrations in the reservoir, with a large aggregation rate $A = 5{,}000$. We compare the asymptotic solutions (3.6, 3.10, 3.15), with a numerical solution of the governing equations, (2.7a-d), at $t = 10$; **a** monomer concentration, c_{b1}; **b** cluster concentration, n_b; **c** inhibitor-particle concentration, h_b; **d** mass per unit area, m_b; **e** typical cluster size $m_b/(c_{b1} + n_b)$

3.2 Dynamic effects

3.2.1 Asymptotic analysis

The previous section considered the steady solutions of the equations governing the reservoir concentrations (2.7a-d). We now investigate how the concentrations evolve to these steady-state values by exploiting the large parameter, A, and analysing the dynamics on several time scales.

For $H > 1$, $H \approx 1$ and $0 < H < 1$, the dynamics on the first two time scales are identical. On a fast time scale, $\tau = At = O(1)$, the concentrations are small and increase due to monomers and inhibitor particles entering the reservoir and clusters forming when two monomers aggregate. Rescaling the concentrations via

$$(c_{b1}, m_b, h_b) = A^{-1}(\tilde{c}_{b1}, \tilde{m}_b, \tilde{h}_b), \quad n_b = A^{-2}\tilde{n}_b, \tag{3.17}$$

the leading-order governing equations (2.7a-d), become

$$\frac{\mathrm{d}\tilde{c}_{b1}}{\mathrm{d}\tau} = 1, \quad \frac{\mathrm{d}\tilde{n}_b}{\mathrm{d}\tau} = \tilde{c}_{b1}^2, \quad \frac{\mathrm{d}\tilde{h}_b}{\mathrm{d}\tau} = H, \quad \frac{\mathrm{d}\tilde{m}_b}{\mathrm{d}\tau} = 1. \tag{3.18a-d}$$

As the inhibitor-particle concentration is small, poisoning is negligible on this time scale. Solving (3.18) subject to the initial conditions, (2.9), we obtain

$$\tilde{c}_{b1} = \tilde{m}_b = \tau, \quad \tilde{n}_b = \frac{\tau^3}{3}, \quad \tilde{h}_b = H\tau. \tag{3.19a-c}$$

The fast $t = O(A^{-1})$ dynamics, (3.19), break down once $\tau = O(A^{1/2})$ because the dominant balance, (3.18), no longer holds. We therefore consider a second time scale, $T = A^{1/2}t = O(1)$. To match to (3.19), the concentrations are $O(A^{-1/2})$, and we therefore rescale via (3.4), which results in the leading-order governing equations

$$\begin{aligned} \frac{\mathrm{d}\hat{c}_{b1}}{\mathrm{d}T} &= 1 - 2\hat{c}_{b1}^2 - \hat{c}_{b1}\widehat{n}_b - \hat{c}_{b1}\hat{h}_b, & \frac{\mathrm{d}\widehat{n}_b}{\mathrm{d}T} &= \hat{c}_{b1}^2 - \widehat{n}_b\hat{h}_b, \\ \frac{\mathrm{d}\hat{h}_b}{\mathrm{d}T} &= H - \hat{c}_{b1}\hat{h}_b - \widehat{n}_b\hat{h}_b, & \frac{\mathrm{d}\widehat{m}_b}{\mathrm{d}T} &= 1 - \widehat{m}_b\hat{h}_b. \end{aligned} \tag{3.20a-d}$$

Comparing (3.5) and (3.20), we see that for $0 < H < 1$, the concentrations approach their steady states, (3.6), in the limit as $T \to \infty$. For initial conditions (2.9), we solve (3.20) using MATLAB's differential equation solver *ode45*, and as shown in Fig. 3, we find excellent agreement with a numerical solution of the full equations, (2.7a-d)

With a large inhibitor input, $H > 1$, the inhibitor-particle concentration is $O(1)$ at the steady state (Sect. 3.1.1), and the flux of inhibitor particles out of the reservoir is significant. Thus, the concentrations evolve to their steady solutions more slowly (than for $0 < H < 1$), and we must also examine dynamics on an $O(1)$ time scale. The concentrations scale via (3.1), and the leading order governing equations give

$$0 = 1 - \tilde{c}_{b1}h_b, \quad 0 = \tilde{c}_{b1}^2 - \tilde{n}_b h_b, \quad \frac{\mathrm{d}h_b}{\mathrm{d}t} = H - h_b - \tilde{c}_{b1}h_b, \quad 0 = 1 - \tilde{m}_b h_b. \tag{3.21a-d}$$

Therefore on the $O(1)$ time scale, the inhibitor-particle concentration increases, and the input of monomers and the formation of clusters are balanced by poisoning of monomers and clusters respectively. Equations (3.21) have solution

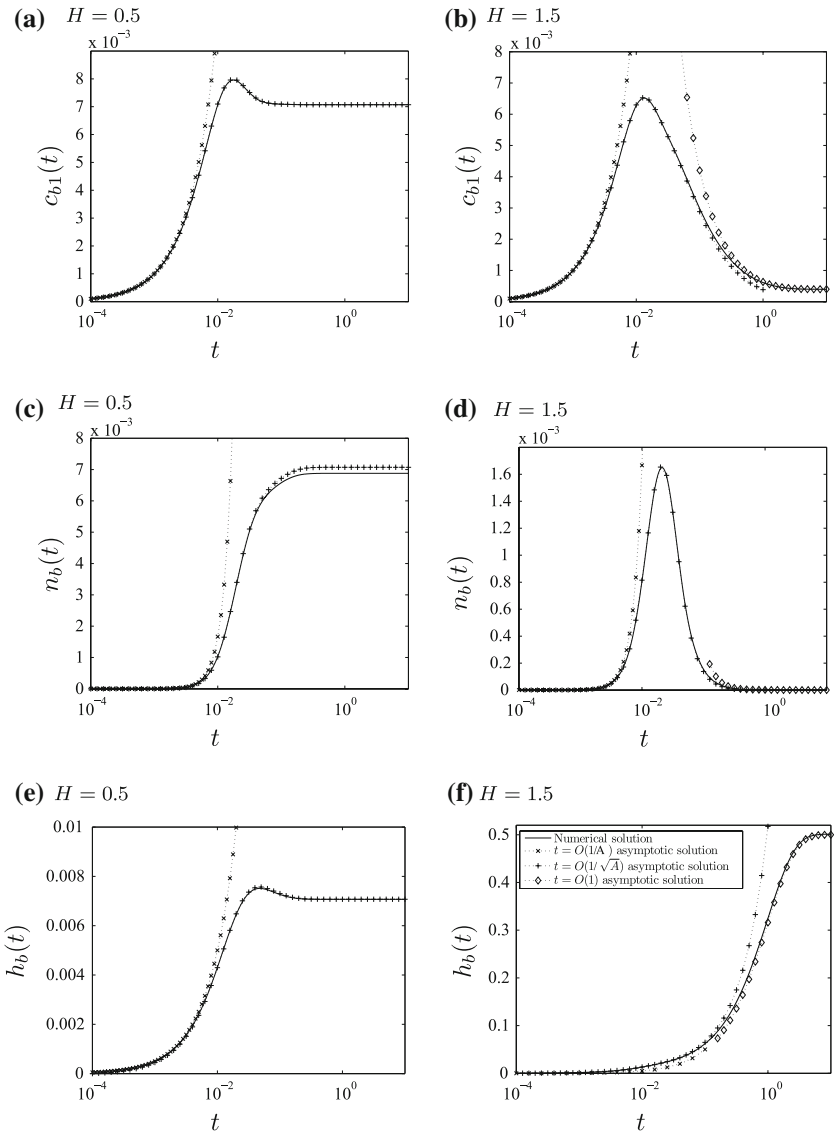

Fig. 3 The evolution of the bulk concentrations in the reservoir. We compare asymptotic and numerical solutions of the governing equations, (2.7a-d), with $A = 5{,}000$ and either $H = 0.5$ (**a**, **c**, **e**) or $H = 1.5$ (**b**, **d**, **f**)); **a**, **b** monomer concentration, $c_{b1}(t)$; **c**, **d** cluster concentration, $n_b(t)$; **e**, **f**) inhibitor-particle concentration, $h_b(t)$

$$h_b = H - 1 + Be^{-t}, \quad \tilde{c}_{b1} = \widetilde{m}_b = \frac{1}{h_b}, \quad \widetilde{n}_b = \frac{1}{h_b^3}, \tag{3.22a-d}$$

where the constant B remains to be determined. To match the dynamics on the intermediate time scale ($t = O(A^{-1/2})$) to those on the $O(1)$ time scale, we require

$\hat{c}_{b1} \to 0^+, \hat{n}_b \to 0^+, \hat{h}_b \to \infty$ and $\hat{m}_b \to 0^+$ as $T \to \infty$. Then (3.20) suggests that $\hat{h}_b \sim (H-1)T$ as $T \to \infty$. Matching these intermediate-time-scale dynamics to the outer solution, (3.22), as $t \to 0^+$, we find $B = H - 1$, which determines the outer solution, (3.22). Considering the scalings for the concentrations on each time scale, we see that the concentrations of monomers and clusters go through transients that are much larger than both their initial conditions and final steady-state values.

For $H \approx 1$, the concentrations also evolve to their steady solutions on an $O(1)$ time scale; in this case, they are scaled via (3.7), and are governed by

$$0 = 1 - \bar{c}_{b1}\bar{h}_b, \quad 0 = 1 - \bar{m}_b\bar{h}_b, \quad 0 = \bar{c}_{b1}^2 - \bar{n}_b\bar{h}_b, \quad \frac{\mathrm{d}\bar{h}_b}{\mathrm{d}t} = \bar{H} - \bar{h}_b + \bar{c}_{b1}^2, \tag{3.23}$$

which reduce to

$$\bar{c}_{b1} = \bar{m}_b = \frac{1}{\bar{h}_b}, \quad \bar{n}_b = \frac{1}{\bar{h}_b^3}, \quad t = \int_0^{\bar{h}_b} \frac{\bar{h}_b'^2}{\bar{H}\bar{h}_b'^2 - \bar{h}_b'^3 + 1}\,\mathrm{d}\bar{h}_b', \tag{3.24}$$

(as matching to the intermediate time-scale dynamics requires that $\bar{h}_b \to 0$ as $t \to 0$). If $\bar{h}_b$ is a root of $\bar{H}\bar{h}_b^2 - \bar{h}_b^3 + 1$, the concentrations satisfy the steady-state equations (3.9); from (3.24), we see that as $\bar{h}_b$ approaches a root of this cubic equation, $t \to \infty$, and therefore the concentrations evolve to their steady-state values on an $O(1)$ time scale according to (3.24).

With $H \approx 0$, the evolution can also be analysed using three asymptotic time scales; however, due to the small inhibitor-particle input, the inhibitor-particle concentration is smaller than in the other cases. At early times, $t = A^{-1}\tau$, the concentrations are scaled via

$$(c_{b1}, m_b) = A^{-1}(\tilde{c}_{b1}, \tilde{m}_b), \quad n_b = A^{-2}\tilde{n}_b, \quad h_b = A^{-4/3}\grave{h}_b, \tag{3.25}$$

and are governed by (3.18, 3.19) (with H replaced by $\breve{H} = A^{1/3}H$, and $\tilde{h}_b$ replaced with $\grave{h}_b$). As before, the fast time scale breaks down once $\tau = O(A^{1/2})$ and we move to the intermediate time scale, $t = A^{-1/2}T$. Here, the concentrations are scaled via

$$(c_{b1}, n_b, m_b) = A^{-1/2}(\hat{c}_{b1}, \hat{n}_b, \hat{m}_b), \quad h_b = A^{-5/6}\acute{h}_b, \tag{3.26}$$

and governed by

$$\frac{\mathrm{d}\hat{c}_{b1}}{\mathrm{d}T} = 1 - 2\hat{c}_{b1}^2 - \hat{c}_{b1}\hat{n}_b, \quad \frac{\mathrm{d}\hat{n}_b}{\mathrm{d}T} = \hat{c}_{b1}^2, \quad \frac{\mathrm{d}\acute{h}_b}{\mathrm{d}T} = \breve{H} - \hat{c}_{b1}\acute{h}_b - \hat{n}_b\acute{h}_b, \quad \frac{\mathrm{d}\hat{m}_b}{\mathrm{d}T} = 1.$$

However, as for $H \gtrapprox 1$, the concentrations evolve to their steady states on an $O(1)$ time scale, with their steady-state scalings (3.12). The evolution is governed by

$$0 = 1 - \breve{c}_{b1}\breve{n}_b, \quad \frac{\mathrm{d}\breve{n}_b}{\mathrm{d}t} = -\breve{n}_b + \breve{c}_{b1}^2 - \breve{n}_b\breve{h}_b, \quad 0 = \breve{H} - \breve{n}_b\breve{h}_b, \quad \frac{\mathrm{d}m_b}{\mathrm{d}t} = 1 - m_b - m_b\breve{h}_b,$$

which reduce to

$$\breve{c}_{b1}=\frac{1}{\breve{n}_b},\quad \breve{h}_b=\frac{\breve{H}}{\breve{n}_b},\quad t=\int_0^{\breve{n}_b'}\frac{\breve{n}_b'^2}{1-\breve{H}\breve{n}_b'^2-\breve{n}_b'^3}\,\mathrm{d}\breve{n}_b',\quad t=\int_0^{m_b'}\frac{\breve{n}_b}{\breve{n}_b-m_b'\breve{n}_b-\breve{H}m_b'}\,\mathrm{d}m_b',$$

(as matching to the intermediate time-scale dynamics suggests that $\breve{n}_b \to 0^+$ and $m_b \to 0^+$ as $t \to 0$). We note that $\breve{n}_b$ approaches a root of $1-\breve{H}\breve{n}_b'^2-\breve{n}_b'^3$ as $t \to \infty$, which corresponds to a solution of the steady state equations (3.14).

3.2.2 Summary of dynamic effects

For $H = 0.5$ and $H = 1.5$, Fig. 3 shows excellent agreement between the asymptotic and numerical solutions of the evolution of the concentrations (from the initial conditions (2.9), to the steady solutions shown in Fig. 2). On the fast time scale ($t = O(A^{-1})$), the concentrations of monomers and inhibitor particles increase due to the flux into the reservoir (Fig. 3a, b, e, f), and the monomers aggregate, which causes the cluster concentration to increase (Fig. 3c, d). As the concentrations of inhibitor particles and clusters increase on time scale $t = O(A^{-1/2})$, more of the monomers become poisoned or aggregate with the clusters, which causes the monomer concentration to decrease (Fig. 3a, b). If the inhibitor-particle input, H, is sufficiently small, more inhibitor particles are taken up in poisoning the monomers and clusters than enter the reservoir, and so the inhibitor-particle concentration reaches a maximum and then decreases to its steady state (Fig. 3e). The cluster concentration remains large in this case, and increases monotonically to its steady state, because the number of clusters that are created by pairs of monomers aggregating is greater than the number that become poisoned (Fig. 3c). With a larger value of H, however, the inhibitor-particle concentration increases monotonically to its steady state, and on a $t = O(1)$ time scale, poisoning causes the cluster concentration to reduce (Fig. 3d). The monomer concentration overshoots its steady state for all H, and depending on the value of H, the concentrations of clusters and inhibitor particles either overshoot their steady state or increase monotonically to their steady state. Note that Fig. 3c clearly shows the $O(A^{-1})$ error in the asymptotic steady solution.

4 Channel solutions

Motivated by the reservoir solutions, we consider the channel dynamics in two asymptotic regimes for H: (i) $H > 1$ where predominantly only monomers and inhibitor particles enter the channel (from Sect. 3.1.1), and (ii) $0 < H < 1$, where monomers, clusters and inhibitor particles enter the channel (from Sect. 3.1.2). We compare solutions with no deposition and with significant deposition, and in the latter case, determine the distribution of deposited monomers and clusters. For both $H > 1$ and $0 < H < 1$, we present numerical solutions and construct asymptotic solutions that capture the region of rapid variation close to the channel entrance. In the limit as $A \to \infty$, the relative sizes of the diffusion, advection, and aggregation terms in the governing

equations (2.7e-h) are the same for the four bulk concentrations (monomers, clusters, inhibitor particles and mass). Asymptotic analysis of similar advection–diffusion–deposition dynamics (but with no aggregation) can be found in references (Woollard et al. 2008; Edwards 1999; Edwards et al. 1999). We do not analyse the $H \approx 1$ and $H \approx 0$ cases; for these cases, the relative sizes of the advection, diffusion and aggregation terms are different for different bulk concentrations which leads to a significantly more complicated asymptotic solution structure, and is beyond the scope of this paper.

The numerical solutions are produced by solving the governing equations, (2.7), using the method of lines. At each time step, we evaluate the right-hand sides of equations (2.7) by approximating the spatial derivatives using second-order accurate central differences, except at the boundaries $x = 1$, $y = 0$ and $y = 1$. Where necessary, we use a variable mesh to resolve the solutions. At the boundaries $x = 1$, $y = 0$ and $y = 1$, we prescribe the first-order derivatives (with respect to x and y respectively) (2.8b-d); we evaluate the derivatives in the governing equations and boundary conditions by creating ghost points and using second-order-accurate central differences. For the time stepping, we again use MATLAB's differential equation solver *ode45*.

4.1 Inhibitor input $H > 1$

4.1.1 With no deposition, $\alpha = 0$

We first consider $H > 1$ and suppose that there is no deposition. Figure 4 shows a numerical solution of the governing equations, (2.7), with $A = 10^4$, $\epsilon = P^{-1} = 0.2$ and $H = 1.5$ at $t = 5$ (by which time the bulk concentrations have reached their steady state). The fluid entering the channel contains small bulk concentrations of monomers and clusters and a large bulk concentration of inhibitor particles. Therefore as the monomers and clusters are advected through the channel, they are poisoned by the inhibitor particles, and the bulk concentrations of monomers and clusters decay rapidly with x (Fig. 4a, b). With a larger inhibitor input, H, monomers and clusters are poisoned faster and their bulk concentrations decay more rapidly with x. Only a small proportion of the inhibitor particles is required to poison all the monomers and clusters, and so throughout the channel the bulk inhibitor-particle concentration is approximately constant and equal to that in the reservoir, $h \approx H - 1$ (results not shown). The bulk concentrations are approximately uniform across the channel width. As in the reservoir with $H > 1$ (Sect. 3.1.1), throughout the channel the typical cluster size is approximately one (results not shown), and the mass per unit area is approximately equal to the bulk monomer concentration (Fig. 4a, c).

At a representative spatial point close to the channel entrance, $x = 0.002$, $y = 1$, Fig. 5 shows the time evolution of the bulk concentrations of monomers, clusters and inhibitor particles to the steady solution shown in Fig. 4. The dynamics are very similar to the reservoir dynamics discussed in Sect. 3.2.2 (Fig. 3b, d, f).

4.1.2 With deposition, $\alpha \neq 0$

Figure 6a–c shows a large-time numerical solution with deposition onto the channel wall, for $A = 10^4$, $\epsilon = P^{-1} = 0.2$ and $\alpha = 100$ (this choice is motivated by the

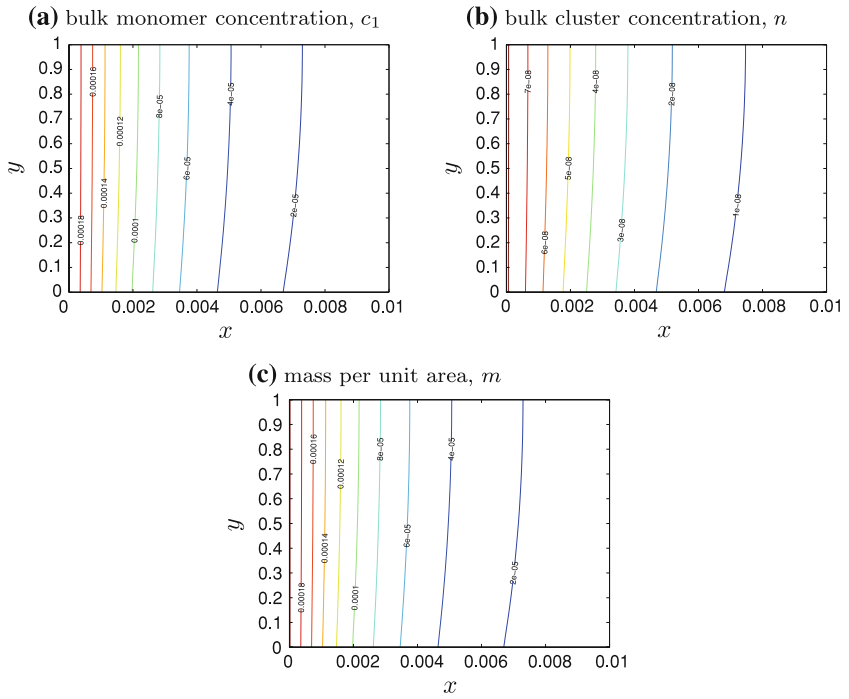

Fig. 4 Numerical solution of (2.7) for the bulk concentrations in the channel at $t = 5$, with a large aggregation rate, $A = 10^4$, and parameters $H = 1.5$, $\alpha = 0$, $\epsilon = P^{-1} = 0.2$, and $D = 1$; **a** bulk monomer concentration, $c_1(x, y)$; **b** bulk cluster concentration, $n(x, y)$; **c** mass per unit area, $m(x, y)$

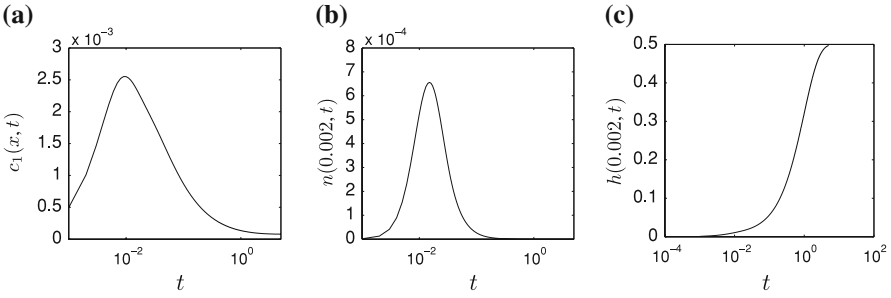

Fig. 5 Time dependence of the bulk concentrations in the channel from a numerical solution of (2.7) with parameters $A = 10^4$, $H = 1.5$, $\alpha = 0$, $\epsilon = P^{-1} = 0.2$, and $D = 1$; **a** bulk monomer concentration, $c_1(0.002, 1, t)$; **b** bulk cluster concentration, $n(0.002, 1, t)$; **c** bulk inhibitor-particle concentration, $h(0.002, 1, t)$

asymptotic analysis in Sect. 4.1.3, which suggests that deposition influences the bulk concentrations provided $\alpha \sim A^{1/2}$). Comparing Figs. 4a, b and 6a, b, we see that deposition only affects the bulk concentrations in a boundary layer next to the channel wall. In the boundary layer, deposition causes the bulk concentrations of monomers and clusters to decay rapidly with x over a shorter axial length of the channel, whereas

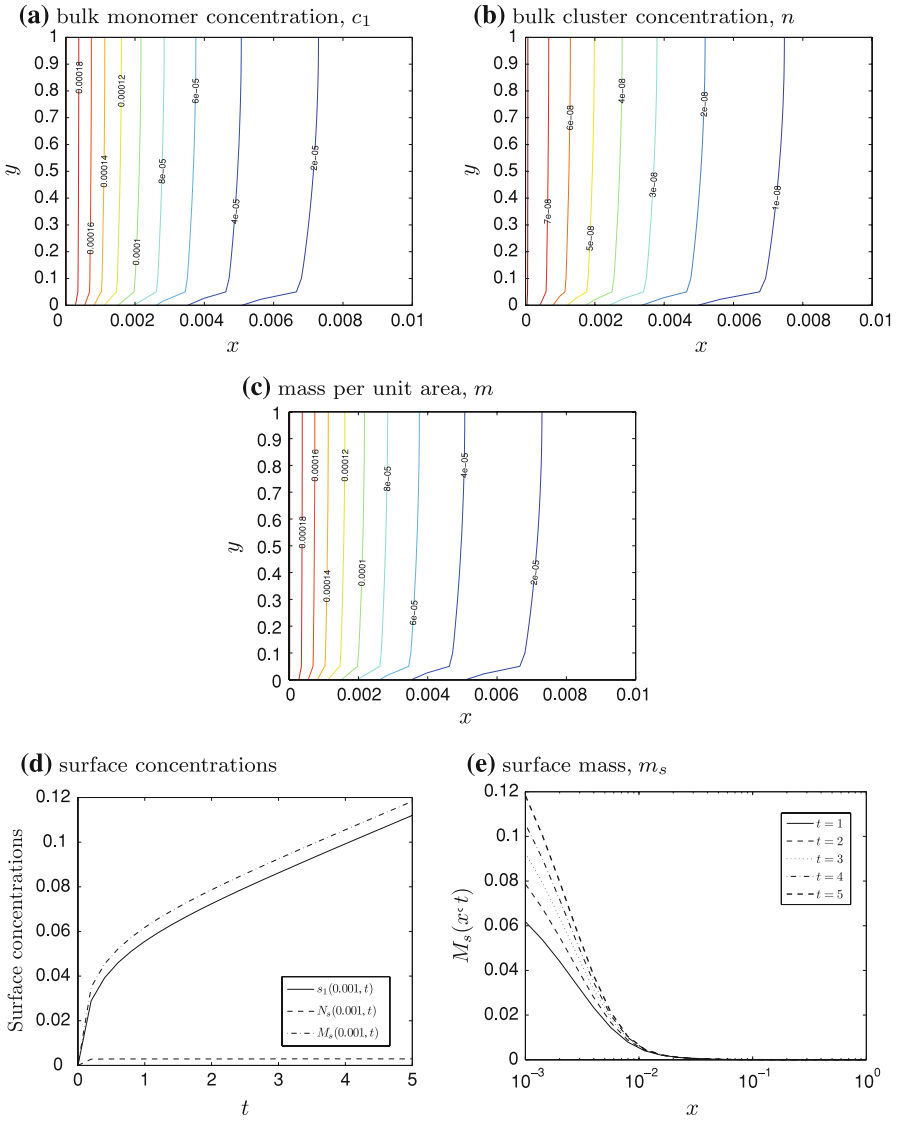

Fig. 6 Numerical solution of (2.7) with a large aggregation rate, $A = 10^4$, and parameters $H = 1.5$, $\alpha = 100$, $\epsilon = P^{-1} = 0.2$, and $D = 1$. The bulk concentrations are shown at $t = 5$ (once equilibrium has been established), and the surface concentrations are shown at $t = 1, 2, 3, 4, 5$; **a** bulk monomer concentration, $c_1(x, y)$; **b** bulk cluster concentration, $n(x, y)$; **c** mass per unit area, $m(x, y)$; **d** time-dependent surface concentrations; **e** surface mass per unit area, $m_s(x, t)$

it leads to slightly larger bulk inhibitor-particle concentrations (results not shown), because there are fewer monomers and clusters for the inhibitor particles to poison.

During the period of the initial increase in the bulk concentrations of monomers and clusters (shown in Fig. 5a, b), monomers and clusters are deposited along the full

length of the channel. Once the bulk concentrations of monomers and clusters have reached their steady state, the surface concentrations increase linearly with time, with their growth rates proportional to the bulk concentrations at the channel wall, (2.7i) (Fig. 6d). Thus, once equilibrium is attained, monomers and clusters predominantly deposit close to the channel entrance, $x = 0$, (Fig. 6e).

4.1.3 Asymptotic steady-state solutions

The numerical solutions show that variations in the steady-state bulk concentrations are confined to a short region close to the channel entrance. We now focus on small x, and exploit large-A asymptotics to examine the structure of the steady solution. We expect the scalings for the bulk concentrations close to the channel entrance to be the same as those in the reservoir; therefore from Sect. 3.1.1, we let

$$(c_1, m) = A^{-1}(\tilde{c}_1, \widetilde{m}), \quad n = A^{-2}\widetilde{n}. \tag{4.1a-c}$$

For small x, it is straightforward to show that the dominant dynamics depend on the relative sizes of ϵ, P and $A^{-1/4}$; considering the physiological parameter estimates, (2.10), we suppose that $\epsilon \sim P^{-1} \gg A^{-1/4}$ and rescale $x = \sqrt{D}\epsilon\tilde{x}/\sqrt{A}$ (where $\tilde{x} = O(1)$ as $A \to \infty$). Thus, in this region, axial advection is negligible and axial diffusion balances aggregation. The leading-order steady-state governing equations, (2.7e-h), become

$$0 = \frac{\partial^2 \tilde{c}_1}{\partial \tilde{x}^2} - \tilde{c}_1 h, \quad 0 = \frac{\partial^2 \widetilde{n}}{\partial \tilde{x}^2} + \tilde{c}_1^2 - \widetilde{n}h, \quad 0 = \frac{\partial^2 h}{\partial \tilde{x}^2}, \quad 0 = \frac{\partial^2 \widetilde{m}}{\partial \tilde{x}^2} - \widetilde{m}h, \tag{4.2a-d}$$

and the bulk channel concentrations equal the bulk reservoir concentrations, (3.3), at $\tilde{x} = 0$. From (4.2c), $h = C_1\tilde{x} + H - 1$, where C_1 is a constant. Before solving for $\tilde{c}_1$, $\widetilde{n}$ and $\widetilde{m}$, we determine C_1 by matching to the $x = O(1)$ solution.

For $x = O(1)$, the steady-state governing equations, (2.7e-h), reduce to

$$0 = \tilde{c}_1 h, \quad 0 = \tilde{c}_1^2 - \widetilde{n}h, \quad 0 = y\left(1 - \frac{y}{2}\right)\frac{\partial h}{\partial x}, \quad 0 = \widetilde{m}h, \tag{4.3a-d}$$

(using scalings (4.1)). Thus, the bulk inhibitor-particle concentration, h, is constant, the remaining governing equations give $\tilde{c}_1 = \widetilde{n} = \widetilde{m} = 0$, and the boundary condition at $x = 1$, (2.8b), is automatically satisfied. Matching to small-x solutions, we find that $h = H - 1$ for all x. We can then use (4.2) to find the remaining small-x bulk concentrations

$$c_1 = m = \frac{1}{A(H-1)} \exp\left(-\frac{x\sqrt{A(H-1)}}{\epsilon\sqrt{D}}\right), \tag{4.4a}$$

$$n = \frac{1}{A^2(H-1)^3}\left[\left(4(H-1)^3 - 1\right)\exp\left(-\frac{x\sqrt{2A(H-1)}}{\epsilon\sqrt{D}}\right) + \left(2 - 4(H-1)^3\right)\exp\left(-\frac{x\sqrt{A(H-1)}}{\epsilon\sqrt{D}}\right)\right]. \tag{4.4b}$$

For $y = O(1)$, there is excellent agreement between the small-x asymptotic steady solutions, (4.4), and the large-time numerical solution of the governing equations (2.7) (results not shown). Note that, as suggested by the numerical solutions in Figs. 4 and 6, the bulk concentrations for $y = O(1)$ are independent of the deposition rate, α.

Next to the channel wall, there exists a boundary layer, $y = O(\epsilon A^{-1/2})$. For $x = O(1)$, the boundary layer solutions are identical to those in the central bulk of the channel, $h = H - 1$, $\tilde{c}_1 = \widetilde{n} = \widetilde{m} = 0$ (for all values of α). At the channel entrance, $x = O(\epsilon A^{-1/2})$, deposition influences the leading-order boundary-layer solutions provided $\alpha = O(A^{1/2})$. In this region, the leading-order governing equations are two dimensional and could be solved numerically; however, we do not pursue this here. With a smaller α, the leading-order bulk concentrations are not affected by deposition and are uniform across the channel width.

4.2 Inhibitor input $0 < H < 1$

4.2.1 With no deposition, $\alpha = 0$

Figure 7 shows a large-time numerical solution of the governing equations, (2.7), with $H = 0.5$, $A = 10^6$, $\epsilon = P^{-1} = 0.05$, and no deposition, $\alpha = 0$. As for $H > 1$ (Fig. 4), the monomers entering the channel at $x = 0$ aggregate with clusters and inhibitor particles as they are advected through the channel, which causes the bulk monomer concentration to decay rapidly with x (Fig. 7a). If H is sufficiently large (for example $H = 0.75$), the dynamics are qualitatively the same as in the $H > 1$ solution: there are enough inhibitor particles present to poison all the monomers and clusters in the initial axial length of the channel, and so only inhibitor particles are present in the remaining length of the channel. In contrast, with a smaller H (for example, $H = 0.5$ shown in Fig. 7), all the inhibitor particles are used up in poisoning the monomers and clusters, and so the bulk inhibitor-particle concentration decays rapidly with x in the initial axial length of the channel (Fig. 7c), and only clusters are present in the remaining portion of the channel (Fig. 7b). Close to the channel wall, monomers, clusters and inhibitor particles are advected more slowly than at the channel centre; therefore, aggregation occurs in a shorter axial length of the channel, and the bulk concentrations of monomers and clusters decay with x more rapidly. As in the reservoir, increasing the input of inhibitor particles leads to a reduction in the mass per unit area and the typical cluster size.

In the channel, the time evolution at a typical point in the flow is qualitatively the same as the evolution in the reservoir which we discussed in Sect. 3.2.2 (Fig. 3a, c, e).

4.2.2 With deposition, $\alpha \neq 0$

Figure 8a–e shows a large-time numerical solution with deposition, for $H = 0.5$, $A = 10^6$ and $\alpha = A^{1/4}$. (We note that this choice of deposition rate is motivated by the asymptotic analysis in Sect. 4.2.3.) As for $H > 1$, deposition causes the bulk concentrations of monomers and clusters to rapidly decay with x close to the wall. As the distance from the channel wall increases, the effect of deposition drops off, and at

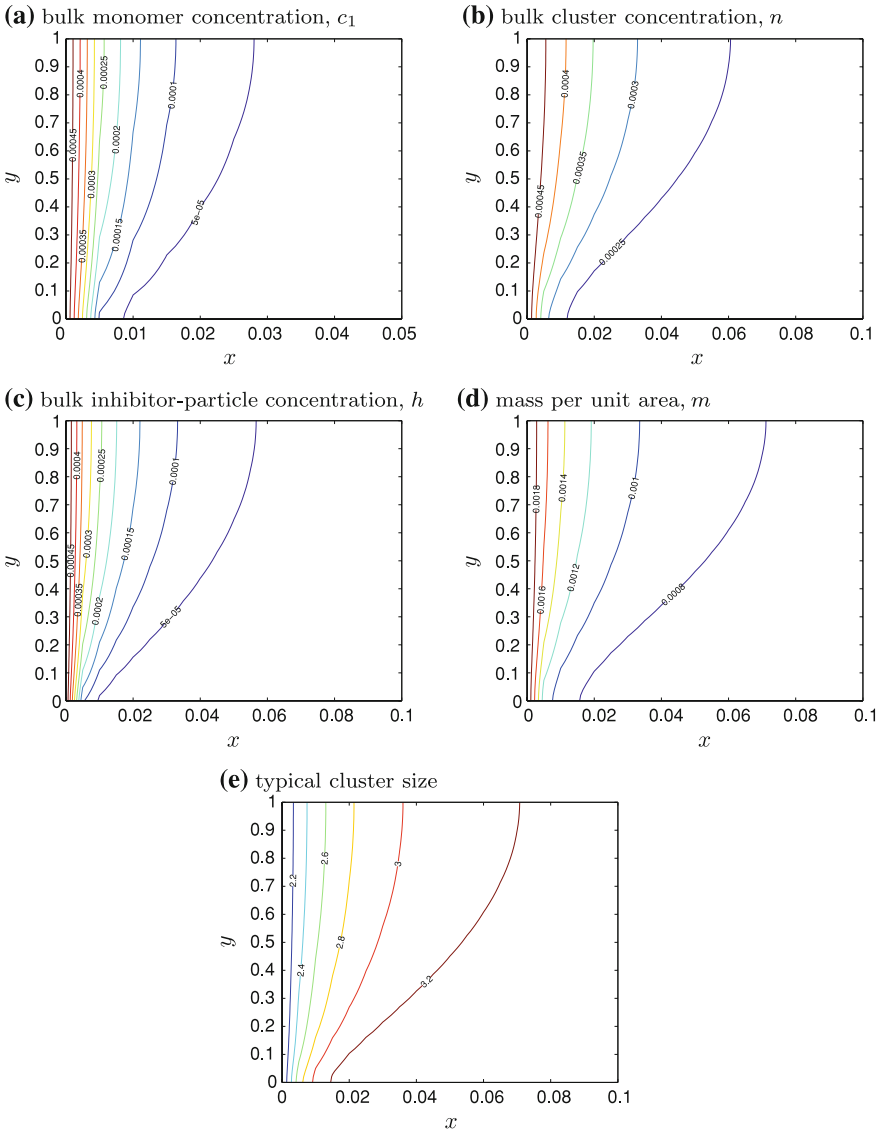

Fig. 7 Numerical solution of (2.7) for the bulk concentrations in the channel at $t = 5$, with a large aggregation rate, $A = 10^6$, and parameters $H = 0.5$, $\alpha = 0$, $\epsilon = P^{-1} = 0.05$, and $D = 1$. The x-scales vary between the graphs to best highlight features of the solution; **a** bulk monomer concentration, $c_1(x, y)$; **b** bulk cluster concentration, $n(x, y)$; **c** bulk inhibitor-particle concentration, $h(x, y)$; **d** mass per unit area, $m(x, y)$; **e** typical cluster size $m/(c_1 + n)$

the channel centre its influence is no longer felt. As for $H > 1$, some monomers and clusters deposit along the full length of the channel wall during the initial transient phase and once the bulk concentrations reach their steady state (shown in Fig. 8a–e), the surface concentrations increase linearly with time (Fig. 8f, g), with their growth rate proportional to the bulk concentrations at the channel wall (from equation (2.7i)).

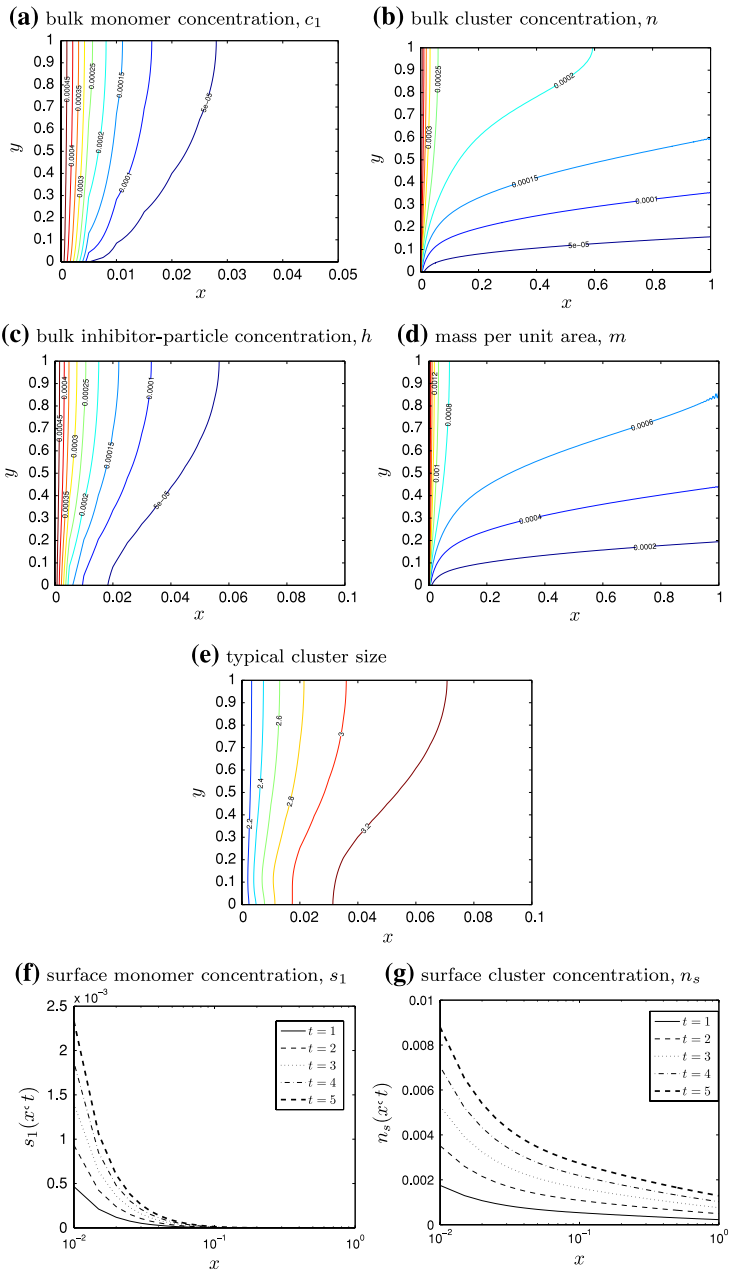

Fig. 8 Numerical solution of (2.7) with a large aggregation rate, $A = 10^6$, and parameters $H = 0.5$, $\alpha = A^{1/4}$, $\epsilon = P^{-1} = 0.05$, and $D = 1$. The bulk concentrations are shown at $t = 5$ (once equilibrium has been established), and the surface concentrations are shown at $t = 1, 2, 3, 4, 5$. The x-scales vary between the graphs to best highlight features of the solution; **a** bulk monomer concentration, $c_1(x, y)$; **b** bulk cluster concentration, $n(x, y)$; **c** bulk inhibitor-particle concentration, $h(x, y)$; **d** mass per unit area, $m(x, y)$; **e** typical cluster size, $m(x, y)/(c_1(x, y) + n(x, y))$; **f** surface monomer concentration, $s_1(x, t)$; **g** surface cluster concentration, $n_s(x, t)$

The steady-state bulk monomer concentration decays rapidly with x in the initial axial length of the channel, and so monomers predominantly deposit in this region (Fig. 8f). If H is sufficiently small, clusters are present throughout the channel at the steady state; clusters continue to deposit along the full channel length (Fig. 8g), and the typical cluster size in the deposited layer increases with x. In contrast, with a larger H, the steady-state bulk cluster concentration rapidly decays in the initial axial length of the channel and so cluster deposition predominantly occurs in this region. In all cases, maximum deposition occurs close to the channel entrance ($x = 0$).

4.2.3 Asymptotic steady-state solutions

As for $H > 1$, the steady-state bulk concentrations vary mainly in the initial axial length of the channel, which enables us to investigate the structure of the solution asymptotically. For small x, we expect the bulk concentrations in the channel to have the same scalings as those in the reservoir (Sect. 3.1.2), thus

$$(c_1, n, h, m) = A^{-1/2}(\hat{c}_1, \widehat{n}, \hat{h}, \widehat{m}). \tag{4.5}$$

It is straightforward to show that the dominant small-x behaviour depends on the relative size of ϵ, P and $A^{-1/8}$. Using the physiological parameter estimates, (2.10), we find it is appropriate to focus on the case $\epsilon \sim P^{-1} \ll A^{-1/8}$. (We note that this regime is consistent with the $H > 1$ assumption that $\epsilon \gg A^{-1/4}$.) For $y = O(1)$, there are three axial asymptotic regimes: for small x, axial diffusion balances advection; for intermediate x, aggregation balances advection; and for $x = O(1)$, aggregation dominates.

In the inner regime, we let $x = D\epsilon^2\hat{x}/P$ (where $\hat{x} = O(1)$ as $A \to \infty$), and we obtain the leading-order balance

$$\begin{aligned} 0 &= \frac{\partial^2 \hat{c}_1}{\partial \hat{x}^2} - y\left(1 - \frac{y}{2}\right)\frac{\partial \hat{c}_1}{\partial \hat{x}}, \quad 0 = \frac{\partial^2 \widehat{n}}{\partial \hat{x}^2} - y\left(1 - \frac{y}{2}\right)\frac{\partial \widehat{n}}{\partial \hat{x}}, \\ 0 &= \frac{\partial^2 \hat{h}}{\partial \hat{x}^2} - y\left(1 - \frac{y}{2}\right)\frac{\partial \hat{h}}{\partial \hat{x}}, \quad 0 = \frac{\partial^2 \widehat{m}}{\partial \hat{x}^2} - y\left(1 - \frac{y}{2}\right)\frac{\partial \widehat{m}}{\partial \hat{x}}, \end{aligned} \tag{4.6a-d}$$

Solving (4.6) subject to the boundary condition (2.8a) at $\hat{x} = 0$, and assuming that the bulk concentrations remain finite as $\hat{x} \to \infty$, we find that the bulk concentrations are constant and equal to the reservoir bulk concentrations (3.6).

As $\hat{x} \to \infty$, the effects of axial diffusion and advection terms diminish; axial diffusion becomes negligible and advection is balanced by aggregation. Thus, with $x = P\bar{x}/A^{1/2}$, the dominant dynamics are governed by

$$\begin{aligned} y\left(1 - \frac{y}{2}\right)\frac{\partial \hat{c}_1}{\partial \bar{x}} &= -2\hat{c}_1^2 - \hat{c}_1\widehat{n} - \hat{c}_1\hat{h}, \quad y\left(1 - \frac{y}{2}\right)\frac{\partial \widehat{n}}{\partial \bar{x}} = \hat{c}_1^2 - \widehat{n}\hat{h}, \\ y\left(1 - \frac{y}{2}\right)\frac{\partial \hat{h}}{\partial \bar{x}} &= -\widehat{n}\hat{h} - \hat{c}_1\hat{h}, \qquad\qquad y\left(1 - \frac{y}{2}\right)\frac{\partial \widehat{m}}{\partial \bar{x}} = -\widehat{m}\hat{h}, \end{aligned} \tag{4.7a-d}$$

and the bulk concentrations are equal to those in the reservoir, (3.6), at $\bar{x} = 0$. For each $y = O(1)$, we solve (4.7) numerically using the method of lines and find good agreement with a large-time numerical solution of the full governing equations (results not shown).

For $x, y = O(1)$, we consider the scalings (4.5), and find the leading-order steady-state governing equations, (2.7e-h), are

$$0 = -\hat{c}_1\widehat{n} - 2\hat{c}_1^2 - \hat{c}_1\hat{h}, \quad 0 = \hat{c}_1^2 - \widehat{n}\hat{h}, \quad 0 = -\hat{c}_1\hat{h} - \widehat{n}\hat{h}, \quad 0 = -\hat{h}\widehat{m}. \quad \text{(4.8a-d)}$$

There are two possible solutions, either $c_1 = h = 0, n \neq 0, m \neq 0$, or $c_1 = n = m = 0, h \neq 0$. We determine the appropriate solution by matching to the numerical small-x solutions (governed by (4.7)). We find that for $H \lessapprox 0.56$ the $x = O(1)$ solution is $c_1 = h = 0, n \neq 0, m \neq 0$; however, for $H \gtrapprox 0.56$, the $x = O(1)$ solution is $c_1 = n = m = 0, h \neq 0$. This is in agreement with the numerical solutions of the full governing equations, (2.7): for large H the inhibitor particles poison all the monomers and clusters in the initial axial length of the channel, and so for $x = O(1)$ the bulk cluster concentration is zero (as in Fig. 4), whereas for smaller H, all the inhibitor particles are used up in poisoning the monomers and clusters, and so for $x = O(1)$, the bulk concentration of inhibitor particles is zero, $h = 0$ (as in Fig. 7). In both cases, all the monomers have aggregated with clusters or been poisoned in the initial axial length of the channel, and so for $x = O(1)$, bulk monomer concentration is zero and the remaining bulk concentrations are constant.

As was the case for $H > 1$, the asymptotic solutions confirm the numerical finding that the deposition does not affect the leading-order dynamics for $y = O(1)$. If $\alpha = O(\epsilon^{-2})$, deposition reduces the bulk concentrations in a boundary layer in the inner region where $\hat{x} = Px/(D\epsilon^2) = O(1)$ and $\hat{y} = Py/(D\epsilon) = O(1)$ (as $A \to \infty$). With a smaller deposition rate, $\alpha = O(A^{1/4})$, deposition does not affect the bulk concentrations in this inner region, but only in the intermediate and final axial regions. Here there is a boundary layer, $y = O(A^{-1/4})$, in which deposition reduces the bulk concentrations of monomers and clusters. If α is smaller than $O(A^{1/4})$ deposition does not influence the leading-order dynamics.

5 Conclusions

We investigate crystal aggregation and deposition in the catheterised lower urinary tract, modelling the bladder as a reservoir of fluid and the urethral catheter as a rigid channel. We assume that monomers and inhibitor particles enter the well-mixed reservoir fluid at a constant rate; the monomers then aggregate to form clusters, and the monomers and clusters are poisoned if they aggregate with an inhibitor particle. The monomers, clusters, and inhibitor particles are advected from the reservoir through the lumen of the channel, where they diffuse and aggregate in the bulk fluid and are deposited on the channel wall. Based on the available physiological parameter estimates, we assume that the ratio between the aggregation rate and the rate at which monomers, clusters and inhibitor particles leave the reservoir and enter the channel, A, is large. We investigate the effect of inhibitor particles on the amount of deposition.

In the reservoir, equilibrium is attained when there is a balance between aggregation, poisoning (inhibition), and the fluxes into and out of the reservoir. Increasing the input of inhibitor particles into the reservoir, H, increases the inhibitor-particle concentration. These inhibitor particles poison the monomers and clusters, and so an increase in H decreases the cluster concentration and the total mass of monomers and clusters per unit area (not including the poisoned monomers and clusters). The relationship between H and the monomer concentration is non-monotonic due to two competing effects: as H increases there are fewer clusters for the monomers to aggregate with, which causes the monomer concentration to increase (this is the dominant effect for $H < 0.5$). On the other hand, as H increases more of the monomers are poisoned which causes the monomer concentration to decrease and is the dominant effect for $H > 0.5$.

As the monomers are advected through the channel, their steady-state bulk concentration decreases due to aggregation with clusters, poisoning by the inhibitor particles and deposition on the channel wall, and thus the bulk monomer concentration rapidly decays over a short axial length of the channel. If H is large, the inhibitor particles poison all the clusters and the bulk cluster concentration also decays rapidly in the initial axial length of the channel and only inhibitor particles are advected through the remainder of the channel. In contrast, with a smaller H all the inhibitor particles are used up in poisoning the monomers and clusters, and so the bulk inhibitor-particle concentration decays rapidly with x, and only clusters are advected through the full length of the channel.

We assume that initially there are no monomers, clusters or inhibitor particles in the reservoir or the channel. As monomers and inhibitor particles enter the reservoir, aggregate and are advected through the channel, the bulk concentrations of monomers, clusters and inhibitor particles increase. In both the reservoir and the channel, the bulk monomer concentration overshoots the steady state for all H, whereas depending on the value of H, the bulk concentrations of clusters and inhibitor particles either overshoot their steady state or increase monotonically to their steady state. During the initial transient phase, before equilibrium is attained, monomers and clusters are deposited along the whole length of the channel. Once the bulk concentrations reach their steady state, the surface concentrations increase linearly with time, with their growth rates proportional to their bulk concentrations at the channel wall. Studying the dynamics using large-A asymptotics, we find that deposition only affects the bulk concentrations in a boundary layer next to the channel wall. If the inhibitor-particle input, H, is sufficiently large, the steady-state bulk concentrations of monomers and clusters rapidly decay with x in the initial axial length of the channel, and deposition predominantly occurs in this region; in contrast, with a smaller H, clusters are present throughout the channel at the steady state and deposition continues along the whole channel length. In both cases, the surface concentrations are greatest at the channel entrance.

We make various simplifying assumptions, the validity of which could be investigated in future work. To make analytical progress, we study the bulk concentration of clusters of two or more particles; however, considering the dynamics of all the different cluster sizes individually could provide further insight. With this formulation, we could extend the model by incorporating fragmentation of the crystal clusters,

and allowing the aggregation and fragmentation rates to depend on cluster size (see Eq. 5.3); such a study would, of course, be primarily numerical. It is also likely that the aggregation rates depend on the local environment (Clapham et al. 1990), for example, on the urine's pH. As the presence of a bacterial biofilm, increases the urinary pH, we could model this phenomenologically by relating the aggregation rates to the local pH. It is also possible that free bacteria within the urine could become trapped within the crystal clusters and further influence the aggregation (Edin-Liljegren et al. 1994).

The model assumes a constant deposition rate; however, it is likely that the deposition rate will depend on cluster size, and may be influenced by the crystals and biofilm present on the catheter surface. It may be more accurate to model aggregation between crystals in the bulk urine and deposited crystals and to consider deposition only on the clean catheter surface. At a later stage of catheter encrustation, the deposited layer will have finite thickness and influence the urine flow, a situation which we investigate in a forthcoming paper (L.R. Band, J.A.D. Wattis, L.J. Cummings and S.L. Waters, paper in preparation).

We ignore spatial variations in the bulk concentrations in the bladder, and we do not consider the catheter's eyelet and balloon, which can also become encrusted (Morris and Stickler 1998). Encrustation of the eyelet and balloon could reduce the bulk concentrations of crystals in the bladder and could reduce the flux from the bladder into the catheter. We also make various simplifications when modelling the inhibition. To make the model more tractable, we ignore the poisoned crystals and assume that they are not deposited on the catheter's surface. We also ignore aggregation between inhibitor particles in the bulk fluid and crystals deposited on the catheter's surface.

All the above model extensions could, in principle, be addressed, although for these more complex mathematical models only numerical solutions would be possible. (The simplifying assumptions made in this paper enable us to make analytical progress, which has lead to a clear understanding of the dominant processes.)

Current literature suggests that the encrusted layer grows due to two mechanisms: by crystals growing within the biofilm, and by crystals growing in the surrounding urine then being incorporated into the biofilm following deposition (Stickler and Morgan 2006; Suller 2005). Although experimental studies suggest that crystals grow more rapidly within the biofilm and that the biofilm provides protection from crystal dissolution (McLean et al. 1991; Clapham et al. 1990), the relative importance of the two mechanisms remains unclear. Our model focuses on the deposition of the crystals which aggregate within the urine. For all parameter values, some crystals are deposited along the full length of the catheter, and deposition is most extensive in the region close to the catheter's entrance. These key features agree with the experimental work by Morris et al. (1999). In contrast, a mathematical model that focused on the crystals that form beneath the biofilm (Siggers et al. discussed in the introduction), found that most encrustation occurs at the opposite end of catheter (farthest from the bladder). These model results (which focus on the two alternative mechanisms) suggest that crystal deposition plays a key role in encrustation and catheter blockage.

Acknowledgments We are grateful to the BBSRC and the University of Nottingham for supporting this project financially. S.L. Waters and J.A.D. Wattis are also grateful to the EPSRC for funding in the form of an Advanced Research Fellowship and a Springboard Fellowship respectively. L.J. Cummings gratefully

acknowledges the hospitality of City College New York, Department of Chemical Engineering, during a sabbatical year 2007–2008. We would like to thank J.H. Siggers, K. Heaton, D.M. Grant, R. Bayston and M.C. Bishop for helpful discussions.

Appendix A: Physiological parameter values

We now discuss the physiological parameter values appropriate for modelling crystal aggregation in urine that is stored in the bladder (the reservoir) and then flows through a catheterised urethra (the channel).

A typical catheter has length $L^* = 0.20\,\mathrm{m}$, and width $2Y^* = 0.016/\pi$ m (corresponding to a catheter size known as 16 F).[2] We take the urine dynamic viscosity to be that of water, $\eta^* = 0.654 \times 10^{-3}\,\mathrm{kg\,m^{-1}\,s^{-1}}$, and the urine temperature to be body temperature, $T^* = 310\,\mathrm{K}$. We assume the bladder volume is constant, and typically $5 \times 10^{-4}\,\mathrm{m^3}$. Thus, the flux of urine into the bladder from the kidneys equals the flux of urine out of the bladder through the catheterised urethra, and we take a typical flux, F^*, to be 1 ml $\mathrm{min^{-1}}$ (or $1.7 \times 10^{-8}\,\mathrm{m^3\,s^{-1}}$) [Cummings et al. 2004; Stickler and Morgan 2006; Morris and Stickler 2001], which corresponds to an average axial velocity of $8.2 \times 10^{-4}\,\mathrm{m\,s^{-1}}$ in the catheter. Equating this physiological average axial velocity with the average axial velocity in our two-dimensional model, $P^*Y^{*2}/(3L^*\eta^*)$, we find that the pressure difference between the reservoir and the external environment is $P^* = 0.050\,\mathrm{Pa}$.

To interpret the dimensional parameters λ^* and Q_1^*, we consider a simplified model in which there is no aggregation, $A^* = 0$. Then, the rate of change of the number of monomers in the reservoir equals the influx of monomers minus the outflux of monomers, *i.e.*

$$\frac{\mathrm{d}}{\mathrm{d}t^*} \int_{V^*} c_{b1}^* \,\mathrm{d}V^* = c_{\mathrm{up}}^* F^* - c_{b1}^* F^*, \tag{5.1}$$

where V^* is the bladder volume, c_{up}^* is the upstream bulk monomer concentration, and F^* is the fluid flux both into and out of the reservoir. As we assume the bladder volume is constant, we simplify (5.1) to find

$$\frac{\mathrm{d}c_{b1}^*}{\mathrm{d}t^*} = \frac{c_{\mathrm{up}}^* F^*}{V^*} - \frac{c_{b1}^* F^*}{V^*}. \tag{5.2}$$

Thus, comparing (5.2) with (2.1a), we find that $\lambda^* = F^*/V^* \approx 3 \times 10^{-5}\,\mathrm{s^{-1}}$, and that we need to estimate the upstream bulk monomer concentration to calculate $Q_1^* = c_{up}^* F^*/V^*$. Mathur et al. (2006) suggest that urine above the nucleation pH contains $2 - 16$ moles of calcium phosphate and $8 - 20$ moles of magnesium struvite per $\mathrm{m^3}$, Thus, assuming that these are suitable estimates for the bulk monomer

[2] The size of a urethral catheter is measured in French units (F), where 1F corresponds to an outer diameter of $1/\pi$ mm (or an outer circumference of 1mm). Catheters typically range from 10 F–28 F.

concentration in the fluid entering the bladder, we take a typical influx bulk monomer concentration to be 10 moles per m^3, and estimate $Q_1^* = 2 \times 10^{20}\,m^{-3}\,s^{-1}$. We represent the presence of citrate by an input of inhibitor particles. Wang et al. (1993) suggest that citrate concentrations in normal urine are between $0 - 4$ moles per m^3 (where 1 mole=6.023×10^{23} particles of unit size). Thus, taking a typical influx bulk monomer concentration to be $2 - 20$ moles per m^3, and a typical influx bulk inhibitor-particle concentration to be $0 - 4$ moles per m^3, the ratio $H = H^*/Q_1^* \in [0, 2]$.

The radius of a crystal monomer is approximately $r_s^* = 5 \times 10^{-10}\,m$ (Wierzbicki et al. 1997), and we determine the diffusion coefficient using the Stokes–Einstein relation $D^* = k^*T^*/(6\pi\eta^* r_s^*) \approx 7 \times 10^{-10}\,m^2\,s^{-1}$ (where Boltzmann's constant $k^* = 1.38 \times 10^{-23}\,m^2\,kg\,s^{-2}\,K^{-1}$). Using the fluid velocity at the channel's centre line, $U^* = P^*Y^{*2}/(2L^*\eta^*)$, the particle Péclet number for the monomers, $P_e^{\text{mon}} = r_s^*U^*/D^* = 7 \times 10^{-6} \ll 1$ and so diffusion dominates over advection. Hence, we use the kernel for diffusion-dominated aggregation derived by Smoluchowski (1916), namely

$$A^* = \frac{2k^*T^*}{3\eta^*}\left(1 + \frac{1}{j^{1/3}}\right)\left(1 + j^{1/3}\right), \tag{5.3}$$

for aggregation between a cluster of j particles and a monomer [see Friedlander (2000) for further details]. To enable analytical progress, we assume the aggregation rate is independent of cluster size and use the kernel for aggregation between a pair of monomers $A^* = 8.7 \times 10^{-18}\,m^3\,s^{-1}$ (from (5.3) with $j = 1$).

References

Amann H, Weber F (2001) On a quasilinear coagulation-fragmentation model with diffusion. Adv Math Sci Appl 11:227–263

Becker R, Döring W (1935) Kinetische Behandlung der Keimbildung in übersättigten Dämpfen. Ann Phys 24:719–752

Bolton CD, Wattis JAD (2004) The Becker-Döring equations with monomer input, competition and inhibition. J Phys A Math Gen 37(6):1971–1986

Burr RG, Nuseibeh IM (1997) Urinary catheter blockage depends on urine pH, calcium and rate of flow. Spinal Cord 35:521–525

Clapham L, McLean RJC, Nickel JC, Downey J, Costerton JW (1990) The influence of bacteria on struvite crystal habit and its importance in urinary stone formation. J Cryst Growth 104(2):475–484

Cummings LJ, Waters SL, Wattis JAD, Graham SJ (2004) The effect of ureteric stents on urine flow: reflux. J Math Biol 49:56–82

Durst F, Ray S, Ünsal B, Bayoumi OA (2005) The development lengths of laminar pipe and channel flows. J Fluid Eng 127:1154–1160

Edin-Liljegren A, Grenabo L, Hedelin H, Pettersson S, Wang YH (1994) Long-term studies of urease-induced crystallization in human urine. J Urol 152(1):208–12

Edwards DA (1999) Estimating rate constants in a convection-diffusion system with a boundary reaction. IMA J Appl Math 63(1):89–112

Edwards DA, Goldstein B, Cohen DS (1999) Transport effects on surface–volume biological reactions. J Math Biol 39(6):533–561

Fozard JA, King JR (2008) Population-scale modelling of cellular chemotaxis and aggregation. IMA J Appl Math 73(1):69–106

Friedlander SK (2000) Smoke, dust and haze. Fundamentals of aerosol dynamics, 2nd edn. Oxford University Press, New York

Guy RD, Fogelson AL, Keener JP (2007) Fibrin gel formation in a shear flow. Math Med Biol 24:111–130
Herrero MA, Rodrigo M (2005) A note on Smoluchowski's equations with diffusion. Appl Math Lett 18:969–975
Laurençot P, Wrzosek D (1998) The Becker–Döring model with diffusion: II Long time behaviour. J Differ Equ 148:268–291
Mathur S, Suller MTE, Stickler DJ, Feneley RCL (2006) Factors affecting crystal precipitation from urine in individuals with long-term urinary catheters colonized with urease-positive bacterial species. Urol Res 34(3):173–177
McLean RJ, Lawrence JR, Korber DR, Caldwell DE (1991) Proteus mirabilis biofilm protection against struvite crystal dissolution and its implications in struvite urolithiasis. J Urol 146(4):1138–42
Morris NS, Stickler DJ (1998) Encrustation of indwelling urethral catheters by Proteus mirabilis biofilms growing in human urine. J Hosp Infect 39:227–234
Morris NS, Stickler DJ (2001) Does drinking cranberry juice produce inhibitory development of crystalline, catheter-blocking Proteus mirabilis biofilms? Br J Urol Int 88:192–197
Morris NS, Stickler DJ, McLean RJC (1999) The development of bacterial biofilms on indwelling urethral catheters. World J Urol 17(6):345–350
Simons S (1992) On the solution of the time-independent equation for the diffusion of coagulating clusters. Phys Lett A 171:172–174
Simons S (1996) On the steady-state equation for particles undergoing simultaneous Brownian diffusion and coagulation. J Phys A Math Gen 29:303–307
Slemrod M (1990) Coagulation-diffusion systems: derivation and existence of solutions for the diffuse interface structure equations. Phys D 46:351–366
Stickler DJ, Morgan SD (2006) Modulation of crystalline Proteus mirabilis biofilm development on urinary catheters. J Med Microbiol 55(5):489–494
Suller MTE, Anthony VJ, Mathur S, Feneley RCL, Greenman J, Stickler DJ (2005) Factors modulating the pH at which calcium and magnesium phosphates precipitate from human urine. Urol Res 33(4):254–260
von Smoluchowski M (1916) Drei Vorträge über Diffusion Brownsche molekular Bewegung und Koagulation von Kolloidteichen. Phys Z 17:557–571
Wang Y, Grenabo L, Hedelin H, McLean RJC, Curtis Nickel J, Pettersson S (1993) Citrate and urease-induced crystallization in synthetic and human urine. Urol Res 21(2):109–115
Wattis JAD (2006) An introduction to mathematical models of coagulation fragmentation processes: A discrete deterministic mean-field approach. Phys D 222(1–2):1–20
Wattis JAD, Coveney PV (1997) General nucleation theory with inhibition for chemically reacting systems. J Chem Phys 106:9122–9140
Wierzbicki A, Sallis JD, Stevens ED, Smith M, Sikes CS (1997) Crystal growth and molecular modeling studies of inhibition of struvite by phosphocitrate. Calcif Tissue Int 61(3):216–222
Woollard HF, Billingham J, Jensen OE, Lian G (2008) A multi-scale model for solute transport in a wavy-walled channel. J Eng Math. doi:10.1007/s10665-008-9239-x